Archimer
https://archimer.ifremer.fr

Quantification of natural microbial methane from generation to emission in the offshore Aquitaine: A basin modelling approach

Torelli Martina [1, *], Kowalewski Isabelle [1], Gervais Veronique [1], Wendebourg Johannes [2], Dupré Stephanie [3], Wolf Sylvie [1], Gout Claude [4], Deville Eric [1]

[1] IFP Energies Nouvelles, 92852 Rueil-Malmaison Cedex, France
[2] Total Exploration Americas, Houston, TX, 77027, USA
[3] Ifremer, Géosciences Marines, 29280 Plouzané Cedex, France
[4] Total, Exploration and Production, Pau Cedex, France

* Corresponding author : Martina Torelli, email address : torellimartina.90@gmail.com

Abstract :

Marine sediments near continental margins contain sedimentary organic matter (SOM) which is subject to the metabolic activity of micro-organisms during early diagenesis resulting in production of biogenic methane. This process occurs at microscopic scale and anaerobic conditions. Here, we apply a new numerical approach to simulate biogenic methane production offshore Aquitaine (Bay of Biscay) where gas seeps have been recently observed as the result of microbial activity. This new approach accounts for: (1) degradation of a labile-SOM fraction to methane, (2) first order kinetics of the thermal degradation of a thermo-labile-SOM fraction into labile fraction at greater burial and (3) decrease of SOM reactivity with time. First, the organic matter is characterized through pyrolysis using Rock-Eval performed on cuttings collected from two wells located within the methane seepage area. The microbial system is fed from a type III continental-derived SOM which is immature (average Tmax < 425°C). The basin model is built and calibrated on seismic and well data. It accounts for the consumption of methane required to precipitate methane-derived authigenic carbonates which are found widely distributed on the seafloor as the result of the anaerobic oxidation of methane during upward migration. A sensitivity analysis is performed on the main model input parameters to quantify their impact on the biogenic gas production and expulsion/migration processes. Results led to a reference scenario for microbial gas production in offshore Aquitaine. With this model the generated methane is predominantly dissolved in water and transported by advective processes. Migration is mainly vertical from the source rock layers to the seafloor and controlled by sediment porosity and strata geometry. Modelling can reproduce natural processes such as gas migration at emission points (gas seeps) which have been previously mapped in the offshore Aquitaine Basin. Our results suggest that the biogenic methane is sourced by a present-day active system with a mean flow rate of 27 Mg/y which is relatively lower than flux modelled during the early Pleistocene reaching up to 41 Mg/y. Calculated total methane lost to the seafloor along the Aquitaine Shelf is in accordance with methane flow rate estimated from in situ measurements and acoustic signatures of bubbling sites, and ranges between 0.87 Tcf/My and 1.48 Tcf/My. Here we propose a new workflow to assess and predict biogenic gas occurrences in offshore environment at the basin scale where gas is sourced by recent continental-derived organic matter. This new approach can help to better assess the

total biogenic methane budget emitted naturally in the shelf area of oceans that may reach the atmosphere with a negative impact on climate and environment.

Highlights

► Innovative 3D basin modelling approach to quantify the budget of biogenic methane in continental shelf areas and calibrated to sea floor emissions ► Sensitivity analysis to determine impact of main parameters on biogenic gas generation and expulsion/migration processes in offshore Aquitaine ► Quantification of methane consumed and stored in authigenic carbonates as function of efficiency of AOM (Anaerobic Oxidation of Methane) ► Methane migration is diffuse and mainly vertical from the source rock layers to the seafloor dissolved in pore water ► Biogenic methane is sourced by an active system with a maximum flow rate modelled during the early Pleistocene

1. INTRODUCTION

Over the last few decades, natural gas has received increasing attention concerning its application as a major and cleaner energy source compared with coal and liquid fossil fuel (Rice and Claypool 1981; Rice 1992, 1993; Whiticar 1994; Kvenvolden 1993; Katz 2011). It is estimated that the annual methane emission from geo-sources only (onshore mud-volcanoes, onshore gas-oil seep, submarine seepage, micro-seepage, geothermal-volcanic manifestations) directly in the atmosphere yields between 27 – 63 Megatons (Etiope and Schwietzke, 2019), with a negative impact on the global climate (IPCC, 2013; Khalil et al. 1993; Judd et al. 2002; Dickens 2004). Even though several estimates have been published over the past years (Hornafius et al. 1999; Judd et al. 2002; Judd et al. 2004; Kvenvolden et al. 2001; Etiope et al. 2008; Etiope and Klusman 2010) our understanding of the methane budget is still uncertain (Etiope and Klusman 2002; Saunois et al. 2016; Schwietzke et al. 2016; Etiope and Schwietzke 2019) especially concerning the potential of natural methane sources from sedimentary basins resulting from microbial activity and/or thermal cracking of buried sedimentary organic matter (Klusman et al. 2000; Etiope and Klusman 2002). It is well accepted that fluid emanations through the ocean floor are ongoing processes represented by characteristic geological features that are widely distributed along near-shore, continental slope and in deep ocean. They include shallow gas accumulations, pockmarks, seeps, mud-volcanoes, authigenic carbonate precipitations and gas hydrates (Jensen 1992; Römer et al. 2012; Skarke et al. 2014; Dupré et al. 2007; Pierre et al. 2017; Hovland et al. 2002; Judd et al. 2002).

Methane generation is the result of Sedimentary Organic Matter (SOM) degradation which takes place at different diagenesis stages (Whiticar et al. 1986; Floodgate and Judd 1992; Whiticar 1999; Schulz and Zabel 2006). In addition to the degradation process of SOM, methane production is controlled by other factors such as temperature, primary productivity, sedimentation rate (Clayton 1992; Judd et al. 2002) and the microorganisms mediating the reaction (Boetius et al. 2000). Biogenic systems can be sourced by poorly-OM layers (TOC < 0.5%) (Clayton 1992). This process is usually observed in deltas where large amounts of sediment are deposited in a short time, containing low continental-OM dispersed in sediments such as the Amazon Delta (TOC ⬚ 0.8%) (Arning et al. 2013) or in the

71   Japanese Pleistocene turbitic sequences of the eastern Nankai Trough (TOC $\square$ 0.5%) (Fujii et al.

72   2016). Methanogenesis in low organic matter sediments is also observed in the Great Australian Bight

73   (TOC < 0.4%) (Mitterer 2010) and in the Woodlark Basin (TOC < 0.4%) (Wellsbury et al. 2002).

74   Therefore, a better understanding of the microbial gas generation process at a large scale is necessary

75   to identify the distribution of methane in the subsurface. In addition, quantifications of natural

76   methane sources and sinks, both at the present day and in the geological past, are of interest to the

77   scientific community working on present and future global climate change (Regnier et al. 2011;

78   Saunois et al. 2016).

79   Numerical modelling is a way to study the interactions of the various geological processes leading to

80   biogenic gas generation, accumulation and migration as these interactions cannot be reproduced in the

81   laboratory given the large spatial dimensions and the slow natural reaction and migration rates.

82   Modelling can be used to critically evaluate and discuss the significance and the role of the main

83   parameters that lead to biogenic gas accumulations. However, it is a challenge to integrate the

84   microscopic processes of methane production at the basin scale. In this paper, we present a

85   quantitative model of the total methane volume generated from microbial activity and emitted offshore

86   Aquitaine (Bay of Biscay, SW France) that is compared with an estimation of emitted methane based

87   on both in situ measurements and acoustic records of a few thousand bubbling sites (Dupré et al. 2020)

88   (Fig. 1). Our approach consists in simulating the biogenic gas generation and migration with a 3D

89   basin model of the study area using a recent numerical implementation for microbial processes

90   modified after Pujol et al. (2016).

91   For biogenic gas generation, our model considers that the initial Total Organic Carbon (TOC) can be

92   partitioned into three different fractions (Fig. 2). A labile fraction called TOClab is composed by the

93   OM that is sensitive to biodegradation from the beginning of deposition (Wallman et al. 2006). A

94   thermo-labile fraction called TOCzlab is composed by the OM that is less reactive and therefore can

95   be preserved in the mineral matrix (Burdige et al. 2007, 2011). The third bio-refractory fraction called

96   TOCbio-ref represents the part of the OM which is later converted to hydrocarbons by thermal

97   cracking when the temperature increases above 80°C (Fig. 2). In our model, this temperature

98   corresponds also to the pasteurization temperature of the micro-organisms (Rice and Claypool 1981;

99   Clayton 1992). Average percentage of TOCbio-reactive for a typical Type II marine OM are: TOClab

100   = 30-40% (Burdige 2007; Wallmann et al. 2006) and TOCzlab = 8-15% (Burdige 2011).

101   Unfortunately, such fractions have not been described for continent-derived terrestrial type III-OM

102   such as found in the Offshore Aquitaine (Michel 2017). It is well known that terrestrial organic matter

103   is mainly composed by higher plants characterized by lower hydrogen and higher oxygenated

104   functional groups contents than marine OM (Burdige 2011; Kamga 2016). When entering in the

105   marine environment, the terrestrial OM is probably already highly altered (Zonneveld et al., 2010).

106   Then, the degradation of OM is followed by an evolution of its molecular composition and its

107   association with the mineral matrix, which tends towards an increasingly refractory nature. As a result,
108   type-III OM dispersed in sediments is less reactive and more thermally-resistant than type II organic
109   matter specially at low temperature (Cowie et al. 1992; Burdige 2007, Kamga 2016). Here, we
110   described the OM based on data available in the literature concerning the geochemical characterization
111   and degradation rate of recent continental-OM (Cowie et al. 1992; Martens and Canuel 1996; Hedges
112   and Oades 1997; Burdige 2007, 2011). However, the fraction of the terrestrial organic carbon
113   preserved in marine sediments is still poorly constrained.

114   The offshore Aquitaine is a unique case study as (1) methane is purely of microbial origin and not
115   related to a thermogenic petroleum system or gas hydrates, (2) there is evidence of persisting methane
116   circulation over time in the form of Methane-Derived Authigenic Carbonates (MDAC) pavements and
117   (3) the quantity of released methane along the shelf at the present day is rather widespread and
118   important (144 Mg/y) (Dupré et al. 2014; 2020; Pierre et al. 2017; Ruffine et al. 2017). In this study,
119   we build a 3D sedimentary model of the offshore Aquitaine that includes a lithospheric model
120   allowing to account for the thermal history of the basin. The model is calibrated with eleven wells that
121   are regionally distributed over the study area (Fig. 3). It also takes into account the MDAC deposits.
122   However, as mentioned above, some parameters related to biogenic gas generation are still uncertain.
123   Thus, we performed a sensitivity analysis to study the impact of these parameters on biogenic gas
124   generation. More precisely, we sampled the parameter space and simulated gas generation and
125   migration for the corresponding set of models to estimate sensitivity indices. Finally, we used the
126   available gas flow rate data to identify a realistic scenario among the sample. The biogenic CH_4 budget
127   for the offshore Aquitaine was calculated for this model, taking the presence of MDAC into account,
128   and compared with locations and quantities of observed natural emissions. According to our results, a
129   gas system originating from only microbial activity can be active over millions of years and can
130   generate important volumes of methane which may either be trapped in the sediments or directly
131   escape to the seafloor, depending on the specific geological settings.

132   The paper outline is as follows. First, the geological setting of the case study is introduced, followed
133   by a description of the data set used to build the 3D basin model. The workflow used to quantify the
134   generated biogenic gas is described in section 4. It encompasses the definition of the 3D sedimentary
135   model, the modelling of the processes of biogenic gas production and migration, and the sensitivity
136   analysis on the uncertain parameters. The application of this workflow to the Aquitaine Basin is
137   described in section 5, followed by some discussions of the results in section 6.

138 ## 2. GEOLOGICAL SETTING

139 *Geodynamic Evolution of the Bay of Biscay*

140 The study area is located in the Bay of Biscay which is bordered by the Armorican Shelf in the North
141 and by the narrow and shallow Basque plateau in the South (Ferrer et al. 2008; Roca et al. 2011;
142 Tugend et al. 2015). The opening of the Bay of Biscay was influenced by the structuration of the
143 Variscan orogeny and is the result of different extensional and compressional cycles (Tugend et al.
144 2014), and notably two rift systems (Ferrer et al. 2008; Tugend et al. 2014): a first North Atlantic
145 rifting phase at the beginning of the Triassic, followed by a second rifting phase during late Triassic to
146 early Jurassic which induced crustal thinning (Boillot et al. 1979) and the formation of intracontinental
147 basins such as the Aquitaine Basin. During the Santonian, the opening of the Atlantic Margin induced
148 a compressional deformation in the southern Bay of Biscay and a weak compressive reactivation in the
149 northern area (Thinon et al. 2001; Tugend et al. 2014). This compressional movement led to the
150 inversion and reactivation of extensional structures which initiated the Pyrenean orogenesis. The
151 major compressional phase was reached during the Eocene and lasted until the end of the Oligocene. It
152 resulted in the accretion of the Pyrenean chain and the formation of the foreland Aquitaine Basin
153 (Tugend et al. 2014). The main target area of our study is the Aquitaine Shelf (Fig. 1) which is part of
154 the offshore Parentis Basin and also represents the main hydrocarbon province of France (Biteau et al.
155 2006). It is filled-up with 15 km of sedimentary cover over a relatively thin crust (Biteau et al. 2006;
156 Bois et al. 1997; Ferrer et al. 2008).

157 *Stratigraphic Framework*

158 This section presents an overview of the Aquitaine Basin stratigraphy. For a more detailed
159 stratigraphic description, readers can refer to Biteau et al. (2006).

160 The sedimentary column is composed at the bottom of a thick evaporitic sequence (anhydrite and salt)
161 deposited in the Triassic during a period of high subsidence.

162 During the Jurassic, deposition was mainly characterized by the development of a westward carbonate
163 shelf: limestones and shale during the Lias, limestones and dolomites during the Dogger. In Oxfordian
164 time, extensional tectonics accelerated which led to the differentiation of the Bay of Biscay into
165 various structural units such as the Parentis Basin where limestone deposition continued, with locally
166 condensed sections until the Kimmeridgian (Biteau et al. 2006). During the late Jurassic the
167 depositional environment became increasingly marine followed by the deposition of the "Mano
168 Dolomite".

169 The Early Cretaceous corresponds to the deposition of undifferentiated marly sediments representative
170 of a shelf environment. During the Aptian, sediments in the Parentis area were characterized by
171 carbonate deposits marking a transgressive period. During the Albian, pelagic shales were deposited,

5

172 including locally clastic turbidites. The Pyrenean compression started during the Upper Cretaceous
173 when the Parentis Basin continued to record a thick sequence of shaly limestones and clays (Biteau et
174 al. 2006).

175 The beginning of the Cenozoic was a period of decreasing sedimentation rates within an open marine
176 context where the continental influence was marked by the presence of numerous marls. During the
177 Oligocene a carbonate shelf developed westwards filled with marly deposits. From the Miocene until
178 today, the area was covered by continental sediments.

179 *Fluid escape features in the Aquitaine Basin*
180 An active fluid system along the Aquitaine Shelf was recently discovered based on previously
181 acquired data collected during recurrent marine expeditions conducted by Ifremer (Pegase98,
182 https://doi.org/10.17600/98040070 and Pelgas2000 to 2011, https://doi.org/10.18142/18). Several echo
183 soundings were recorded in the water column caused by gas bubbles located at 140-220 m water depth
184 (Dupré et al. 2014). This fluid system has been further assessed during the GAZCOGNE1 (Loubrieu
185 2013) and GAZCOGNE2 surveys (Dupré 2013). It extends over 375 km² along the Aquitaine Shelf,
186 with 2612 bubbling sites (Dupré et al. 2020) (Fig. 1).

187 Molecular and isotopic analysis on gases (δD and $\delta^{13}C$) revealed that these fluids are composed of
188 almost pure biogenic methane (> 99.94% mol of the gases) generated from CO_2 reduction (Ruffine et
189 al. 2017) without any link to the thermogenic sources from the Parentis Basin. Associated with these
190 gas escapes, authigenic carbonate pavements are widely developed above and below the sub-seafloor
191 over 375 km² (Pierre et al. 2017; Dupré et al. 2020). The bubbling sites, as well as the authigenic
192 carbonates, are located east of the continental shelf break (Fig. 1) and no such activities were observed
193 along the slope or inside the erosional canyon where the uppermost Pleistocene layers were removed
194 (Michel et al. 2017; Dupré et al. 2020). Plio-Pleistocene and Holocene deposits are potential
195 candidates for the source layers from which the microbial methane is generated (Dupré et al. 2020) as
196 they record high sediment and organic matter supply (Cremer 1983).

197 Several scenarios for the source rock layers were investigated by Michel (2017). Based on regional
198 horizon geometry from seismic data, geochemical evidence from Rock-Eval analysis and potential
199 migration pathways, the source rocks for microbial methane are most likely located within the Upper
200 Pleistocene progradational units (Michel 2017). However, based on the regional thermal gradient
201 (Biteau et al. 2006) and temperature ranges for microbial activity (Katz 2011), it cannot be excluded
202 that deeper source rocks may also contribute to the microbial gas generation (Dupré et al. 2020).

203 The isotopic signature of the carbonate cements demonstrates that these sedimentary features are the
204 result of Anaerobic Oxidation of Methane (AOM) (Pierre et al. 2017). The precipitation of the
205 methane-derived authigenic carbonates takes place within the Sulphate-Methane Transition Zone

206 (SMTZ) which corresponds to an oxic-anoxic boundary located in most cases below the seafloor at

207 variable depth (Boetius et al. 2000).

208 These shallow-water seeps in the Aquitaine Basin are very different from classical deep-sea cold water

209 seeps. As proposed by Pierre et al. (2017a) this system could be compared with seeps found along the

210 northern U.S. Atlantic Margin (Pierre et al., 2017b) where methane emission sites have been

211 discovered at 50-1700 m water depth as the result of freshwater discharge to the seafloor more than

212 100 km away from the coast (Cohen et al. 2010; Skarke et al. 2014). Indeed, based on the oxygen

213 isotopic signature of bulk carbonate and aragonite cements, MDAC from the Aquitaine Shelf

214 precipitated from a mixture of seawater and freshwater as the result of submarine groundwater

215 discharge at the seafloor (Pierre et al. 2017). This fluid system is highly dynamic. Therefore, it is

216 easily influenced by the depth variations of the AOM and SMTZ, and possibly by the amount of

217 groundwater discharge at the seafloor and along the slope where the erosion within canyons partially

218 removed the uppermost sources of the biogenic methane.

219 This process linked to the precipitation of MDAC could be the reason why the location and migration

220 of the methane seeps occur east of the shelf break. Indeed, emission sites are mainly located along a

221 narrow band oriented N-S parallel to the Aquitaine Shelf with highly variable amount of emitted gas

222 or MDAC deposits (Dupré et al. 2020). The fluid activity is more intense in the southern part of the

223 basin compared with the northern part and the same differences are observed for the MDAC deposits

224 which are widely distributed in the southern part and more localized in the northern area (Dupré et al.

225 2020). Note that both thickness and initial age of the MDAC are still unknown. Based on Dupré et al.

226 (2014; 2020) gas migration pathways are mainly controlled by sedimentary processes (indicated by

227 precipitation of MDAC) rather than by tectonic activity (faults). As MDAC pavements can have a

228 major control on the gas migration and they represent a major sink for methane, we accounted for the

229 AOM in our model. The study area is located in the northern part of the Aquitaine Basin where the

230 flow rate of methane emitted into the water column is estimated to be around 35 Mg/y (Dupré et al.

231 2020) (Fig. 1b).

232 **3. DATA SET**

233 *Source rock samples*

234 The geochemical characterization of the organic matter was done through Rock-Eval analysis

235 (Espitalié et al. 1977; Espitalié et al. 1985; Lafargue et al. 1998). Based on previous studies (Michel

236 2017; Dupré et al. 2020) and on the regional geothermal gradient (Biteau et al. 2006), it is accepted

237 that the main target zone for biogenic gas production in our system is located at shallow depths in the

238 Plio-Pleistocene progradational systems. However, deeper source rocks may take part in the

239 generation of microbial methane (Dupré et al. 2020). Thus, we collected samples between 595-1530 m

240 bsf in the Plio-Pleistocene to upper Miocene sediments (Table S1). Exploration wells usually target

241 reservoirs and not source rocks that are deeper so that samples from cores are rarely available at these

242 depths. Nevertheless, 20 cuttings were collected from two exploration wells (Pelican-1, Pingouin-1)

243 located at the external shelf area (Fig. 3). Cuttings are broken pieces of rocks derived from drilling

244 processes. They are used to make a record of the investigated rock with a depth uncertainty of around

245 ±15 m related to recovery operation. Considering that the minimum thickness of the source rock layers

246 defined in our model is greater than 15 m, this uncertainty was assumed acceptable for our case study.

247 All samples were washed, desalted and prepared in accordance with the procedure applied at IFPEN

248 (Lafargue et al. 1998; Behar et al. 2001).

249 *Maps and well data*

250 Interpreted seismic horizons from the top basement to Cretaceous were taken from the OROGEN

251 project (funded by Total, BRGM, CNRS & INSU), and from base Miocene to seabed from Ortiz et al.

252 (2020), and they were used to construct a 3D model of the Bay of Biscay (Table 1). The interpretation

253 of the three main units composing the Plio-Pleistocene progradational system are given in Michel

254 (2017) (U1, U2 and U3, Table 1). Eleven exploration wells were drilled by Elf Aquitaine in the area of

255 interest during the 60s, 70s and 80s. They are mainly located along the coast and along the shelf-break

256 area as shown in Fig. 3. Measurements performed at these wells provide data used to calibrate the

257 basin model as described in the next sections: facies logs, uncorrected Bottom Hole Temperatures

258 (BHT) for 7 wells (see Fig. 7), vitrinite reflectance for 6 wells (Fig. 8) and pressure at two wells (Fig.

259 S1).

260 Correction of BHT measurements can be more than 10% above the actual measure (Deming 1989).

261 Because no information about the mud circulation time was found in the composite logs, it was

262 decided to correct these measurements by adding 10% of the measured value and to consider an

263 uncertainty of ±10%.

264 Vitrinite reflectance data yield information about the maximum temperature experienced by the

265 sediments (Jones and Edison 1979; Oberlin, 1980; Carr 2000). The measurements however were

266 reported without any description of the sample type (e.g. dispersed organic matter, coal, extracted

267 kerogen), therefore these measurements remain questionable. Pressure measurements indicate

268 hydrostatic gradients which have been used to determine the average water salinity in the offshore

269 Aquitaine Basin.

4. METHODS

Rock Eval analysis to determine biogenic gas generation potential

The Rock-Eval technique is widely used in academia and petroleum industry to determine the hydrocarbon potential, type and maturity of source rocks (Espitalié et al. 1977; Espitalié et al. 1985; Lafargue et al. 1998; Behar et al. 2001). This type of analysis is applied either on bulk rock samples (Espitalié et al. 1977) or on isolated kerogens or coals (Behar et al. 2001). The Rock-Eval technique consists in a thermal analysis of the sample through two analytical steps with specific temperature programs: a pyrolysis under inert atmosphere (N_2) followed by a combustion of the residual sample under an oxidative atmosphere (air). The hydrocarbons are detected using a Flame Ionization Detector. The CO_2 and CO released by the pyrolysis and oxidation phases are continuously swept towards an infrared detector (Espitalié et al. 1985). A small amount of crushed source rock (about 70 mg) or isolated kerogen (5 to 30 mg) is usually exposed in the pyrolysis oven to a temperature of 300 °C for 3 minutes before applying a heating rate at 25°C/min up to 650 or 800°C respectively. But since our samples are recent sediments containing immature organic matter, we applied a lower isotherm and the samples were heated at an initial temperature of 200°C as proposed in Baudin et al. (2015). During the pyrolysis cycle, three peaks are detected. The S1 peak obtained during the pyrolysis isotherm determines the amount of free hydrocarbons in the samples (mg HC/g of rock). The S2 peak obtained during the pyrolysis heating rate corresponds to the hydrocarbons released by thermal cracking (mg HC/g of rock). This S2 peak represents the remaining hydrocarbon potential of a source rock. The S3 peaks partly correspond to the amount of CO and CO_2 released during thermal cracking (mg CO or CO_2/g of rock). The main parameters calculated from Rock-Eval data are: Total Organic Carbon (TOC%) representing the total organic carbon content, Hydrogen Index (HI) (mg HC/g TOC) and Oxygen Index (OI) (mg CO_2/g TOC). These parameters are used to determine the type (e.g. lacustrine, marine or continental) and the maturity of organic matter. Another parameter is also used as a proxy for the maturity of a source rock: Tmax (°C) that corresponds to the temperature measured at the peak of S2.

Basin modelling

Sedimentary model

The static model of the Aquitaine Basin was built based on present-day topography (Ortiz et al. 2020) and 13 subsurface horizons that were derived from seismic interpretations (Table 1) (Michel 2017; Ortiz et al. 2020; M. Roger, personal com.). The surface of the model area is around 2800 km² (Fig. 3), divided horizontally into grid blocks of 1x1 km². The model also includes the methane-derived authigenic carbonates distribution at the sub-seafloor (Dupré et al. 2020). The eleven exploration wells were used to cross-check the depth maps (Fig. 3). Finally, each isopach was associated with a

9

304   lithofacies map (Fig. 3). The facies distribution was obtained by well log correlation, with an

305   additional uppermost MDAC layer for wells located within the sub-seafloor MDAC area (i.e. Pelican-

306   1 and Fregate-1) (Figs 3, 7 and 8). The paleo-bathymetry for each horizon was defined in accordance

307   with literature (Desegaulx and Brunet 1990; Brunet 1994). In order to more accurately model the

308   processes of biogenic gas generation, the vertical resolution was increased in the main zone of

309   biogenic gas production. Thus, the shallower strata from the Miocene to the Plio-Pleistocene layers

310   were subdivided into several sub-layers (Table 1). The Miocene layer, which presents an average

311   thickness of 600 m, was subdivided into six 100 m-thick sub-layers. The Plio-Pleistocene units U2 and

312   U3 were also refined. The U2 unit was subdivided into seven sub-layers with an average thickness of

313   60 m. The U3 unit was subdivided into eight sub-layers with a thickness of 90 m. No sub-layering was

314   applied to the U1 unit as its thickness is only around 100 m. Finally, we applied a lithological switch

315   at two uppermost layers in order to account for MDAC deposits, that mimics the appearance of these

316   particular lithofacies after deposition. The final static model is composed of 39 depositional events and

317   one litho-switch event (Fig. 3, Table 1).

318   *Boundary Conditions*

319   In order to model the thermal evolution through time, a lithosphere model was created with varying

320   bottom boundary conditions. The three main elements that characterize the lithosphere (upper crust,

321   lower crust and upper mantle) were taken from publications (Artemieva and Thybo 2013; Brunet

322   1994; Brunet 1997). The base of the upper mantle is assumed to be the base of the model, defined by

323   the 1333°C mantle isotherm representing the Lithosphere-Asthenosphere Boundary (LAB) and was

324   digitized from Artemieva and Thybo (2013). Two rifting events experienced by the Bay of Biscay

325   (Ferrer et al. 2008; Tugend et al. 2014; Brunet 1994; Desegaulx and Brunet 1990) were defined to

326   model heat flow variations in the geological past. The rifting is initiated from a McKenzie-type crustal

327   model with an instantaneous (less than 20 My) stretching of the lower and upper crust (McKenzie

328   1978). Then, the subsidence of the basin is simulated using extension coefficients (β-factor) from

329   Brunet (1997): β = 1.2 for the Triassic rift event and β = 1.4 for the Upper Jurassic rift event.

330   The upper thermal boundary is defined as a surface temperature map at the top of the model for each

331   geological time step using the *Paleo-latitude calculator for Paleoclimate study* from van Hinsbergen

332   et al. (2015) and the equivalent diagram from Wygrala (1989) which require paleo-latitudes of the

333   basin over time. Since temperatures at the sea-bottom are usually much cooler compared with onshore

334   environments at the same latitude (Dembicki 2016), the sea bottom surface temperature was corrected

335   for paleo-bathymetry using the method described in Toole (1981). This resulted in a series of

336   temperature maps, one for each geological event, that were imposed at the top of the model and that

337   account for the changing latitude and bathymetry of the basin.

338 *Biogenic source rock definition*

339 Biogenic gas generation of a given source rock occurs between 10 and 100°C (Katz et al. 2011) and is

340 determined as a function of thermal gradient (°C/km) and sedimentation rate (m/My) (Schneider et al.

341 2016). An optimal heating rate at deposition time ranges between 7°C/My and 18°C/My (Clayton,

342 1992) (Fig. 4).

343 The thermal gradient and sedimentation rate maps were computed by the TemisFlow® simulator and

344 multiplied to determine the heating rate maps at deposition time for each layer (Fig. 5a-c). These maps

345 were then converted into biogenic potential index maps that determine the areas in which any OM may

346 be converted to microbial CH_4 (Fig. 5d).

347 Five potential source rock layers in the Plio-Pleistocene series and one potential source rock in the

348 Miocene sediments presented optimal conditions for biogenic gas generation. Their input geochemical

349 parameters (e.g. TOC and HI) were taken from the Rock-Eval analysis (Table S1).

350 ***Concepts of modelling biogenic gas generation and migration processes***

351 Published OM degradation models (Westrich et al. 1984; Janssen 1984; Middelburg 1989; Middelburg

352 et al. 1996; Canuel and Martens 1996; Boudreau and Ruddick 1991; Robinson and Brink 2005; Arndt

353 et al. 2013) are the results of experimental laboratory studies, performed at human time scales and at

354 specific thermal conditions. A basin model however needs to represent the time span of the entire

355 geological history of a basin and its thermal evolution. A general modelling approach is needed that

356 accounts for the main biogenic gas production processes but that can also be applied at different

357 geological space and time scales.

358 Our modelling approach considers the total initial Sedimentary Organic Matter (SOM) is composed of

359 TOClab, TOCzlab and TOCbio-ref. The labile TOClab is (Eq. 1, Fig. 2) the part of the OM that is

360 immediately degraded at the moment of deposition according to the degradation law of Middleburg

361 (1989) which is a function of OM reactivity (R_{bio}) and microbial activity ($\mu(T)$) (Eq. 1). This model

362 describes an exponential decrease of the OM with depth and time and leads to a strong degradation in

363 the first few meters of the sedimentary column. This shallow depth is challenging in basin simulators

364 where the vertical resolution of layers is usually in the range of tens to hundreds of meters. In addition,

365 all hydrocarbons generated or migrated in the uppermost layer are assumed lost to the surface. Under

366 these conditions, only the fraction of TOClab at greater depth would be capable of generating biogenic

367 gas. In order to account for a higher fraction of the biodegradable OM, a thermogenic source of labile

368 TOC is introduced in our conceptual model (Burdige 2007; Burdige 2011). It is represented by the

369 thermo-labile part (TOCzlab) of the initial TOC and corresponds to the OM that can be trapped and

370 protected in the mineral matrix during the first stages of diagenesis (Burdige 2011). When temperature

371 increases, TOCzlab can turn into labile OM which is sensitive to biodegradation. This process releases

372　new labile compounds later in time and results in an additional generation of biogenic gas at greater

373　depth. The transformation of TOCzlab is modelled using a first-order kinetic cracking scheme (Eq. 2).

374　For a continental-derived OM, composed mainly by waxes of higher plants (Largeau and

375　Vandenbroucke 2007; Kamga 2016), the generation of methane at low temperature is mainly the result

376　of the degradation of the aliphatic portions (*e.g.* long fatty acids) (Kamga 2016) considered as the most

377　thermo-labile compounds with low activation energy. The third and last fraction of the initial TOC

378　(TOCbio-ref) is bio-refractory and corresponds to the TOC fraction that is used in traditional

379　petroleum systems analysis. TOCbio-ref is not sensitive to microbial activity and is converted into

380　hydrocarbons by thermogenic cracking reactions only. In this study, TOCbio-ref values are derived

381　from Rock-Eval analysis (see Table 3).

382　Thus, the total initial SOM is defined as the sum of these three fractions (Fig. 2):

383　**Total Initial SOM** $= \boldsymbol{TOCbio\text{-}ref} + \boldsymbol{TOClab} + \boldsymbol{TOCzlab}$

384　TOClab evolution through time follows a continuous degradation law (Eq. 1):

$$\frac{\partial \text{TOClab}}{\partial t} = -\, Rbio * (abio + t)^{-b} * \mu(T) * \text{TOClab} - \frac{\partial \text{TOCzlab}}{\partial t} \quad (1)$$

385　where R_{bio} represents a dimensionless calibration parameter linked to the sedimentary environment. A

386　default value of 0.16 is derived from Middelburg (1989). a_{bio} is the apparent initial age of the OM

387　(Ma), t the time of the degradation process (Ma) and b is equal to 0.95 (Middelburg 1989). $\mu(T)$ (°C) is

388　the temperature dependent function of microbial activity derived from Belyaev et al. (1983).

389　TOCzlab degradation is defined by a first order kinetic reaction (Eq. 2):

$$\frac{\partial \text{TOCzlab}}{\partial t} = -k(T) * \text{TOCzlab} \quad (2)$$

390　where reactivity k is defined by the Arrhenius law (Eq. 3):

$$-k(T) = A * e^{-\frac{Ea}{RT}} \quad (3)$$

391　T represents the temperature (K), Ea the activation energy (kJ mol^{-1}), R the universal gas constant

392　(8.3144621 J.mol^{-1}.K^{-1}) and A the frequency factor (s^{-1}).

393　The final generated biogenic gas is derived from the transformation of the labile organic carbon

394　fraction whose biogenic CH$_4$ generation rate (τbio) (Eq. 4) is defined as:

$$\tau bio = -\, \frac{mCH4}{mC} * sbio * \frac{\partial \text{TOClab}}{\partial t} \quad (4)$$

395   where m_{CH_4} = methane molar mass, m_C = carbon molar mass and s_{bio} = stoichiometric coefficient

396   controlling the amount of organic carbon which is converted to microbial methane.

397   In conclusion, biogenic methane is directly generated by the labile TOC fraction following two steps

398   (Fig. 2): first, the labile TOC fraction is transformed into methane, and then the thermo-labile TOC is

399   transformed at greater depth into labile TOC that is afterwards converted into additional methane.

400   Once the biogenic gas is generated, it is subject to the following processes (in order of priority): (1)

401   adsorption by the organic matter following the Langmuir law, which quantifies the capacity of the OM

402   to adsorb methane as a function of temperature and pressure; (2) dissolution in formation water

403   following an equation of state (EOS) which is a function of pressure, temperature and salinity, and

404   subsequent advective transport in the water phase (Duan et al. 1992); (3) migration in a separate vapor

405   phase following multi-phase Darcy's law.

406   Biogenic gas can also be accumulated in structural or stratigraphic trap in a vapor phase, or as a solid

407   phase in the form of gas hydrates (Brothers et al. 2014; Johnson et al. 2015; Skarke et al. 2014). In the

408   Aquitaine Basin, however, temperature and pressure conditions are not conducive to gas hydrate

409   deposits (Dupré et al. 2020). The absence of hydrates over geological time is also confirmed by our

410   numerical simulations.

411   *Quantitative sensitivity analysis*

412   As mentioned in the introduction, the values of the model parameters, and especially those describing

413   the biogenic gas generation process, are uncertain. Sensitivity analysis can be performed to estimate

414   the impact of these parameters on the modelled processes and to determine those that are the most

415   critical. This can help to better understand the processes involved in the biogenic gas production and

416   migration and to simplify the calibration process by focusing on the relevant parameters.

417   Here we performed a variance-based global sensitivity analysis to quantify the influence of the

418   parameters on the output of interest (Sobol' 1990). More specifically, input parameters are considered

419   to be independent random variables with given probability distributions. Indices are then computed

420   that quantify the impact of the parameter uncertainty on the output variance. The main (or first-order)

421   effect measures the part of the output variance explained by the parameter alone. It ranges between 0

422   and 1. The total effect, as defined in Homma and Saltelli (1996), estimates the global sensitivity of the

423   output to the parameter. The difference between the total and main effects corresponds to interactions

424   between the studied parameter and some other parameters.

425   The estimation of the main and total effects requires knowing the value of the output of interest for a

426   very large number of models. To avoid such a computational overburden, we consider here meta-

427   models that mimic the simulator. More precisely, we generate a sample of the parameter space and

428   perform the corresponding simulations. This provides a set of basin models, the training set, that is

429   used to approximate the relationship between the input parameters and the output of interest, providing

430   fast estimations of this output for any parameter values (Wendebourg 2003; Feraille and Marrel 2012).

431   If these estimations are accurate enough, they can replace the calls to the simulator during the

432   computation of the sensitivity indices. To check the quality of the meta-model estimations, we

433   consider here an additional sample of the parameter space, independent from the training set, and

434   compare the output simulated values for these new models with those predicted by the meta-model.

435   The resulting errors are gathered in the R2 correlation index (see Gervais et al. (2018) for more

436   details).

437   This workflow has already been used in a variety of contexts. In what follows, meta-models are built

438   by kriging interpolation, and are combined with reduced-basis decomposition to predict the spatial

439   distribution of properties in the basin as described for instance in Gervais et al. (2018).

5. RESULTS

Organic Matter Characterization

442   As mentioned above, to characterize the OM we collected cuttings at depths ranging from 595 to 1530

443   m from the Pelican-1 and Pingouin-1 wells located in the offshore Parentis Basin. At the same depth

444   and formation interval, the two wells showed different TOC values (Table 1S). Pingouin-1 is

445   characterized by a very low OM content which an overall decrease with depth ranging from 0.44% in

446   the shallower Plio-Pleistocene to 0.32% TOC in the Miocene. The Pelican-1 well shows higher OM

447   content, with TOC values principally ranging from 0.44% to 0.47% respectively from the top Plio-

448   Pleistocene to the base Miocene. Only one sample (PELICAN-7) is characterized by a higher TOC

449   value of around 10.35% which is probably due to the presence of black OM in vitrinite residues

450   already observed and described in Michel (2017). Otherwise, the samples show OI values between

451   ~240 and 500 mgCO$_2$/gTOC and very low HI ($\leq$ 55 mg HC/gTOC) suggesting an altered continental-

452   derived OM (Fig. 6). A mean Tmax value of 420°C indicates that the OM is immature.

Thermal and pressure regime

454   Calibration of present-day temperatures was obtained by modifying thermal conductivities of

455   lithologies in each strata in accordance with those given in Pasquale et al. (2011). Calibration results

456   are shown in Figure 7. A lithospheric model (section 4) constrained the thermal evolution of the basin

457   through time which was calibrated with vitrinite reflectance data from 6 wells (Fig. 8). Note that in

458   this study, we do not model any deeper thermogenic petroleum systems as those known in the offshore

459   Parentis Basin as we focus on Cenozoic strata within which the biogenic gas source rocks are found.

460   According to the calibrated model, the Miocene layer reaches its maximum temperature between 32

461 and 45°C at the present day. These temperatures also correspond to the microbial activity peak and

462 optimal conditions for the generation of microbial gas (Katz et al. 2011). Note also that vitrinite

463 measurements were reported without any description of the rock samples from which they were taken

464 adding to the uncertainty of the final paleo-temperature history.

465 Pressure measurements indicate some overpressure in the basin: Pelican-1 encountered an

466 overpressure of 6.28 MPa at 3125 m in a shaly horizon, Antares-1 encountered a small overpressure of

467 1.78 MPa at 2056 m (Figure 1S). Hydrostatic pressure gradients depend on salinity. The water

468 composition offshore Aquitaine is highly variable, probably related to the presence of large salt

469 accumulations and extensive diapirism. Salinities encountered in Pelican-1 show a mean value of 65

470 g/l ± 15 at 1823-1860 m depth (Paleocene), a mean value of 150/180 g/l at 2500 m (Aptian), and

471 values up to 145 g/l at 2800 m (Barremian). Salinities from the Antares-1 well show lower values at

472 similar depths (56 g/l at 2567 m). Despite such a high variability of water salinity, pressure calibration

473 was achieved with a mean water salinity of 50 g/l.

474 *Sensitivity Analysis on biogenic gas generation*

475 As mentioned previously, the parameters describing the biogenic gas generation are not completely

476 known for continental-derived terrestrial type III-OM in the Aquitaine Basin. We thus performed a

477 sensitivity analysis on 7 input parameters likely to have a significant impact on biogenic gas

478 generation in the offshore Aquitaine: TOC_{lab}, TOC_{zlab}, R_{bio}, Ea, μ(T), s_{bio} and water salinity.

479 Ranges of kinetic parameters are based on published data for a type III organic matter (Middelburg

480 1989; Hedges and Oades, 1997; Martens and Canuel al. 1996; Burdige 2007, 2011) and on previous

481 modelling work of biogenic gas generation (Ducros and Wolf 2014; Ducros et al. 2015). As presented

482 in Burdige (2011 and reference therein), the activation energy (Ea) for recent organic matter can vary

483 between 50 to 130 kJ/mol. In our case study, biogenic gas generation is favorable when Ea is

484 comprised between 80-110 kJ/mol. Higher or lower value prevent the biogenic gas generation. We

485 therefore reduced the range proposed in Burdige (2011) as proposed in Table 2. Here, we did not

486 consider the frequency factor (A) of the TOC_{zlab} kinetics (Eq. 3) as a critical parameter. Indeed, it is

487 well known that, for the same reactivity, variations in Ea can be compensated by A (Peters et al.

488 2018). In accordance with previous kinetic studies (Behar et al. 1997; Dieckmann 2005; Schenk et al.

489 1997) we fixed A and varied Ea in the range of published data to find an optimal kinetic law for

490 TOC_{zlab}. However, in order to more accurately describe the degradation of a recent type-III OM and

491 reduce uncertainty, further research should focus on the analytical assessment of the molecular

492 composition of a recent continental-derived organic matter.

493 The perturbation of the μ(T) function is performed through the variation of the temperature

494 corresponding to the peak of maximum activity instead of varying the function as presented in Table

495 2. Water salinity was included in the sensitivity analysis to assess its impact on methane dissolution

496 rather than on the final amount of generated gas. The ranges of variation of all the critical input

497 parameters are given in Table 2.

498 To estimate the sensitivity indices, a Latin Hypercube sample of 100 models was generated (McKay et

499 al. 1979) and used to get first qualitative results.

500 Since the migration of microbial gas evolves as a function of the total amount of generated gas (SQG,

501 Fig. 9), special attention was given to the sensitivity of SQG to the uncertain parameters. Figure 10

502 shows the value of SQG for the 100 models of the sample as a function of Ea, s_{bio} and R_{bio}. We can

503 observe a negative correlation between SQG and the activation energy (Ea), as well as a positive

504 correlation for both s_{bio} (Fig. 10a,b) and low values of R_{bio} (Fig. 10c). No clear trend can be observed

505 for the other parameters.

506 The results of the variance-based sensitivity analysis on SQG are presented in Figure 11. The meta-

507 models used to compute these total and main effects were derived from the 100 models and quality-

508 checked using 50 additional models. Parameters Ea, s_{bio} and R_{bio} appear to be the most influential on

509 SQG, while the proportion of labile versus thermo-labile compounds in the OM (TOClab and

510 TOCzlab) seems to have only a limited impact. This may be related to the quite small range of

511 variation chosen for these fractions.

512 If we now consider in more details the spatial distribution of parameters Ea, s_{bio} and R_{bio} total effect on

513 SQG in the layers (Fig. 12), we can observe some variability depending on the source rock horizon.

514 The impact of Ea is strongest in the Miocene source rock and decreases in the shallower Plio-

515 Pleistocene layers (Fig. 12). This is probably due to degradation rates for the thermo-labile part of the

516 OM that increase with temperature (Eq. 3) and thus with depth. As a result, the variability of Ea has

517 more impact at greater depth. The same trend is visible for s_{bio}: the influence on SQG increases with

518 depth, with a higher impact on the deeper Miocene source rock compared with the uppermost Plio-

519 Pleistocene sediments (Fig. 12). This result is probably linked to the higher organic carbon availability

520 in the deeper source rock, derived from the total transformation of both TOClab and TOCzlab, which

521 is then converted to biogenic methane as function of s_{bio} (Eq. 4). The results for R_{bio} show the opposite

522 behavior: the impact is strongest in the uppermost layers where TOClab is the most sensitive to

523 degradation, and small in the deeper layers (Fig. 12).

524

525 *Scenario for microbial gas generation*

526 In our model, each source rock layer, from the deeper Miocene to the shallower Plio-Pleistocene, is

527 defined by a constant TOCbio-ref determined from Rock-Eval analysis (Table 3). The degradation

16

528   laws for the labile compound and the kinetic laws for the thermo-labile fraction are identical for each

529   source rock layer. We use the estimation of the gas flux in the northern area identified by Dupré et al.

530   (2020) to constrain these laws. More specifically, the difference between the total mass of generated

531   gas and the total mass of gas in place (either adsorbed, dissolved or free) provides us an estimation of

532   the amount of gas lost at the seafloor, and thus an estimation of the gas flux which can be compared to

533   the flux measured by Dupré et al. (2020) in the northern area. The optimal value among the set of

534   models is obtained for the input parameters values given in Table 2 ("This study" column). We can see

535   that it requires a low activation energy of 83 kJ/mol, which is necessary to activate the thermo-labile

536   TOC fraction at low temperatures as in the case of the Plio-Pleistocene source rocks. This model is

537   considered in what follows as our reference scenario.

538   With this scenario, the average per-area amount of generated gas is 78 kg/m² (Fig. 13) which amounts

539   to 25.5 Gt/My when integrated over time along the entire area of ~1188 km² (Fig. 14). The highest

540   microbial gas amount is generated by the upper Miocene source rock which reached its highest

541   temperature (~ 32°C) at the present day. Methane is first generated by the initial labile fraction during

542   early diagenesis but continues to be generated by other labile molecules derived from the

543   transformation of TOCzlab with increasing temperature. The area of maximum generation is localized

544   along the shelf edge where the sediment thickness is the highest resulting in both higher burial and

545   temperature. Generation decreases along the upper slope where no fluid activity has been identified

546   (Dupré et al. 2020) (Figs. 1, 14). Part of this generated gas is adsorbed to the source rock, or dissolved

547   in the pore water, or trapped as a free gas when saturations are high enough. As shown in Figure 13,

548   biogenic gas is mainly present in the system as dissolved in water. Formation water is almost always

549   under-saturated with respect to CH_4 and a free methane phase is minimal in the uppermost layers

550   mainly at the shelf break (Fig. 13d). Dissolved gas moves driven by hydrodynamic gradients. As

551   compaction is the main driving force, water flow is mainly vertical and therefore methane flux is also

552   mainly vertical, from the source rock to the seafloor. However, flow in the uppermost strata is

553   impacted by MDAC deposits which prevent gas to easily escape to the seafloor. The modelled gas

554   migrates upwards along a narrow N-S oriented strip near and east of the shelf break (Fig.14) where gas

555   generation rate and sediment permeability are most favorable.

556   Once the fluid reaches the seafloor, methane is exsolved as a free gas phase. Our results suggest that

557   gas seeps at the seabed may be principally linked to gas diffusion close to the water/sediment interface

558   rather than from large quantities of free gas migrating to the surface. Considering the difference

559   between the total mass of generated and in place gas (either adsorbed, dissolved or free), we estimate

560   that the amount of gas lost at the seafloor is 0.91 Gt/My over an area of ~107 km² which corresponds

561   to the gas flux in the northern area modelled after Dupré et al. (2020) (Fig. 14).

562 **6. DISCUSSIONS**

563 *Cumulative volume of released microbial methane at the seafloor in the Aquitaine Shelf*

564 Dupré et al. (2020) estimated an amount of emitted methane over the Aquitaine Shelf of 144 Mg/yr

565 based on measurements from local bubbling sites (Ruffine et al. 2017) and acoustic water column

566 signatures of escaping gas bubbles. Our study area is restricted to the northern Aquitaine Shelf (see

567 location in Fig. 1b) and corresponds to 1.88 Tcf/My (Trillion Cubic Feet per million years) (Dupré et

568 al. 2020).

569 Our model indicates a total mass of generated microbial methane of 25.5 Gt/My over 5.53 My

570 corresponding to the time since the beginning of the generation process. At the maximum generation

571 depth (mean depth ~1100 m), the deeper source rock is at P-T conditions of ~ 10 MPa and ~ 35°C

572 where CH_4 density is 72 kg/m^3 using the AGA8 equation of state (ISO 12213-2 2006; Starling and

573 Savidge 1992) (Fig. 15). Thus the total volume of generated gas is $3.55*10^{+5}$ Mm^3/My (equivalent to

574 12.8 Tcf/My).

575 At the water depth range of emission sites, P-T conditions are 2.6 MPa and 10°C resulting in a gas

576 density of 19.7 kg/m^3 (Fig. 15). Based on a gas loss of 0.91 Gt/My, we can estimate the cumulative

577 volume of emitted gas as $4.63*10^{+4}$ Mm^3/My (equivalent to 1.62 Tcf/My).

578 MDAC pavements represent a sink of CH_4. At the edge of the Aquitaine Shelf, they are associated

579 with microbial methane seeps which are oxidized in the Anaerobic Methane Oxidation zone to CO_2

580 (Pierre et al. 2017). During upward migration, the generated methane meets the SO_4^{2-} of the downward

581 diffusing seawater in the Sulphate-Methane Transition Zone where it is consumed by the activity of

582 methanotrophic archea with SO_4^{2-} reducing bacteria (Boetius 2000; Conrad 2005; Thauer 2010; Lash

583 2015) in anoxic conditions. Note that we did not account for the sulfate-reduction of organic matter as

584 it is one of the process less likely to induce local authigenic carbonate precipitation compared to the

585 AOM (Paull and Ussler 2008). In addition, extensive precipitation of MDACs within the subsurface, is

586 usually related to SMTZ occurring at shallower sub-bottom depths (e.g. < 20 mbsf) (Paull and Ussler

587 2008 and reference therein) which can be the case of the Bay of Biscay (Pierre et al. 2017, Dupre et al.

588 2020). Here, we assume that in the Bay of Biscay the AOM is the driving process for MDAC

589 precipitation.

590 The AOM redox reaction can be described as the net reaction between seawater sulfate and methane

591 (Eq. 6):

592 $$\mathbf{CH_{4(aq)} + SO_4^{2-} \rightarrow HCO_3^- + HS^- + H_2O_{(l)}} \qquad \mathbf{(6)}$$
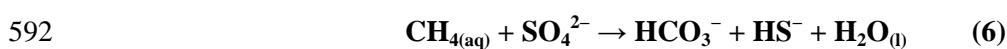
593 The dissolved inorganic carbon (bicarbonate) generated in the STMZ under anaerobic conditions
594 increases alkalinity that promotes carbonate precipitation resulting in the formation of authigenic-
595 carbonate (Eq. 7) (Boetius 2000; Regnier et al. 2011; Lash 2015).

$$2HCO_3^- + Ca^{2+} \longleftrightarrow CaCO_3 + CO_2 + H_2O \qquad (7)$$
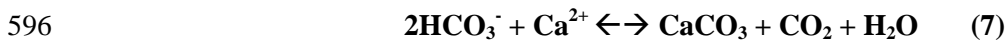
597 This process is a widespread diagenetic reaction along modern continental margins (Reeburgh 2007,
598 Lash 2015) where part of the generated methane is consumed before it reaches the seafloor (Regnier et
599 al. 2001). Therefore, methane oxidation during upward migration should also be taken into account to
600 model biogenic gas processes. However, the integration of this process in basin modelling is
601 complicated by the fact that the AOM thickness is very small, around 2 m within the STMZ, and
602 occurs at variable shallow depths.

603 Based on the current knowledge from the offshore Aquitaine (Dupré et al. 2020), we can estimate the
604 average amount of CH_4 consumed through the AOM. Using a mass balance approach, the CO_2
605 "trapped" in MDAC is 43% of the total molar mass of $CaCO_3$. The exact thickness of the MDAC
606 outcropping and sub-cropping is unknown but with information from seismic data (Fig. 1, Dupré et al.
607 2020), we can estimate a variable thickness of 2 to 10 m which is discontinuous along the shelf.
608 Considering an extent of MDAC of 200 km² (Fig. 14), we can determine an average volume of
609 MDAC. Assuming an average thickness of 5 m for the MDAC, we can estimate the amount of CO_2
610 stored in the carbonates which corresponds to the total amount of CH_4 consumed through AOM.

611 The total mass of consumed CH_4 (mCH_4) through the AOM can be defined as (Eq. 8):

$$mCH_4 = \rho*V*f \qquad (8)$$

613 where ρ is the $CaCO_3$ density (2700 kg/m³), V is the $CaCO_3$ volume (m³) and f is the molar fraction of
614 CO_2 trapped as MDAC equal to 43%. Note that we are assuming that all CO_2 both in the system and
615 trapped in the MDAC derives from methane oxidation only.

616 To convert the total CH_4 mass (Eq. 8) to total gas volume, we consider that at the emission water depth
617 the gas density is 19.7 kg/m³ (Fig. 15) resulting in $5.89*10^{+4}$ Mm³ of CH_4 (2.06 Tcf) that is trapped in
618 MDAC. This means that 23% of the uprising methane is consumed through AOM resulting in a
619 reduced total emission rate of 1.25 Tcf/My. Note that if we consider a lower limit of MDAC thickness
620 of 2 m, the emission rate is 1.48 Tcf/My corresponding to 9% of CH_4 consumed through AOM. In
621 contrast, a higher thickness of 10 m results in 0.87 Tcf/My of microbial CH_4 emitted at the seafloor,
622 corresponding to 46% of CH_4 trapped in MDAC.

623 *Modelled present-day flow rates of microbial methane*

624 The modelled hydrodynamic regime of the northern Aquitaine Basin is shown in Figure 16. During

625 compaction, porosity loss induces vertical water expulsion (Fig. 16a, b). In our model, most of the gas

626 is dissolved in the formation water (Fig. 13) in the upper layers that are characterized by

627 unconsolidated sediments with high porosity (modelled values between 50 and 60%) (Fig. 16a, b).

628 Therefore, we can approximate the methane flux to the vertical water flux. We also observe that the

629 low porosity of MDAC at the seafloor acts as a barrier preventing the water to circulate easily up to

630 the water-sediment interface (Fig. 16a). Migration and expulsion processes are then controlled by the

631 hydrodynamic regime of the upper part of the basin in which methane migrates to the seafloor as a

632 function of sediment geometry, permeability and water flux.

633 Our model indicates methane in a free gas phase whenever gas saturation is reached in the water. This

634 condition is sensitive to the amount of free water in the layer, P-T conditions and amount of generated

635 gas. Basin modelling grids are limited by their spatial resolution. Layer thickness and cell size can

636 impact the amount of free water in the system. Gas saturation is reached when gas generation or

637 pressure conditions are high enough to exceed the solubility threshold or when layer thickness is

638 sufficiently small which reduces the amount of free water. In our model, we observe that the majority

639 of the gas is dissolved in water due to gas saturation that is decreasing during upward migration

640 caused by AOM. Indeed, in the Aquitaine Shelf, MDACs represent the main sink for CH_4 and

641 therefore imply that gas remains dissolved in water up to the seafloor where it diffuses due to

642 changing thermodynamic conditions at the seafloor. Given the high permeability of the upper

643 unconsolidated sediments (Fig. 16 b), we can assume that the total gas released at the present day is

644 proportional to the water flow through the uppermost layer.

645 Due to the absence of capillary pressure, it is not possible to accumulate hydrocarbons in the

646 shallowest layer. Thus, we calculated the water flow through the second-last layer as follows (Eq. 9)

$$Methane\ Flux = \frac{[CH4]tf - [CH4]ti}{tf - ti} \quad (9)$$

647 where ti corresponds to the last geological event defined in the model (0.14 Ma) and tf to the present

648 day. As shown in Figure 16, gas is migrating upward to the seafloor along the Aquitaine Shelf edge

649 but no such activity is observed on the slope (Dupré et al. 2020; Michel et al. 2017). Variations of

650 methane concentration in water have been computed for several grid cells and integrated over the

651 northern study area (Fig. 1b) which yields an average methane flow rate of 27 Mg/y (Fig. 17). This

652 number has the same order of magnitude as the estimated methane flow rate of 35 Mg/y from in situ

653 flow rate measurements and acoustic data (Dupré et al. 2020).

654 In our model, the total mass of emitted methane yields a methane flux of 23 mgCH$_4$/m²/y over the

655 northern Aquitaine surface (Fig. 1b). Present-day methane flow rats have also been compared with

656 paleo-flow rates. We computed concentration changes of dissolved gas in water between the

657 deposition of the first Plio-Pleistocene source rock at 2.87 Ma and the following geological event (Δt =

658 0.23 My). The average amount of emitted methane in that time interval reaches 11 Mg/y

659 corresponding to 9.8 mgCH$_4$/m²/y. In contrast, the deposition of the last source rock layer at 1.76 Ma

660 and the following geological event (Δt = 0.19 My) results in a methane flow rate of 41 Mg/y

661 corresponding to 35 mgCH$_4$/m²/y, which turns out to be the maximum modelled methane flux through

662 the seafloor. Therefore, present-day flow rates are relatively smaller because all the source rocks are

663 already deposited and the more "mature" Miocene source rock had already generated a large part of its

664 labile potential resulting in a higher flux in the past compared to what we currently observe. This

665 result is probably due to the absence of sediments above the Plio-Pleistocene source rocks during time

666 of deposition (1.76 Ma), where the gas can easily escape through the seafloor compared to the present

667 day where gas migration is controlled by an overburden and its permeability. Thus, gas migration over

668 time along the offshore Aquitaine Shelf edge evolves as a function of variable generation and

669 sedimentation rates.

670 Note that in our study, we did not take into account a probable input from a Holocene source rock as

671 proposed in Dupré et al. (2020). Indeed, in our model, the Holocene layers are too shallow (between

672 150 to 200 m of water depth along the shelf) to act as a probable biogenic source rock. We can also

673 assume that its contribution to the final cumulative volume of generated/emitted gas would be low

674 compared to any deeper source rock.

7. CONCLUSIONS

676 This study presents for the first time an attempt to quantify the total amount of emitted biogenic gas at

677 the seafloor over time, applied to the Aquitaine Shelf. Along with a calibrated basin model,

678 geochemical results from Rock-Eval and quantitative sensitivity analysis, we propose a model for the

679 evolution of the microbial methane system in the sediments of the offshore Aquitaine Basin.

680 A global sensitivity analysis based on meta-models helped to identify the most critical parameters for

681 gas generation. Given the uncertainty ranges for the input parameters, methane production appears

682 mainly controlled by the reactivity of the OM rather than by the relative percentage of labile and

683 thermo-labile compounds. The final amount of generated microbial methane strongly depends on the

684 deposition age of the source rock. In our model, all source rocks depleted their thermo-labile fraction

685 that is defined by a low activation energy. Only the shallower and more recent Plio-Pleistocene source

686 rocks still have a labile potential to generate biogenic gas compared to the older and deeper Miocene

687   source rock that is totally depleted. However, a dedicated analytical assessment of the reaction kinetics

688   and reactivity of the OM is required in order to more accurately assess OM degradation.

689   The generated gas is mainly present in the system as dissolved in water migrating vertically until it is

690   finally released as a separate gas phase at the seafloor. Migration pathways are controlled by sediment

691   permeability and by maximum generation rates along the shelf. This system seems to be active since

692   the first source rock was deposited in the Messinian, with a mean modelled methane flow rate of 11

693   Mg/y until the deposition of the last source rock during the early Pleistocene where it reaches a

694   maximum emission rate of 41 Mg/y when all source rocks were deposited without any further

695   sedimentation and the gas was easily released at the seafloor. Modelling results also show that present-

696   day methane flow rates (27 Mg/y) are in the same order of magnitude than flow rates estimated from

697   in situ flow rate measurements and acoustic data (35 Mg/y) (Dupré et al. 2020). Our results confirm

698   that the absence of a seal at the top of the system resulted in continuous methane emission over time

699   along the offshore Aquitaine Shelf edge and CH_4 flow rate intensities evolved as function of microbial

700   methane generation and sedimentation rates.

701   Our modelling approach demonstrates that a gas system originating from only microbial activity can

702   be active over millions of years generating significant methane volumes that depend on the specific

703   geological setting. In our 3D model, the mass of generated gas over time corresponds to 25.5 Gt/My of

704   biogenic CH_4. The difference between the total mass of generated methane and the total mass still in

705   place (in either adsorbed, dissolved or free state) yields a loss of 0.91 Gt/My. However, part of this gas

706   is not directly released at the seabed but rather oxidized into CO_2 through AOM during upward

707   migration. Based on MDAC thickness variation of 2 - 10 m and assuming that all CO_2 present in the

708   system is sourced by methane oxidation only, we could determine an average amount of consumed

709   CH_4 through AOM varying between 9% and 46% of the initial generated methane volume. Thus, the

710   average volume of emitted gas over time along the Aquitaine Shelf ranges between 0.87 Tcf/My and

711   1.48 Tcf/My. This result demonstrates that if we want to better understand and estimate the total

712   amount of emitted methane and its impact on the ocean/atmosphere carbon budget, we need to account

713   for (1) the total amount of generated gas, (2) the total amount of trapped gas in the system and (3) the

714   total amount of consumed gas through the AOM.

715   In this study, we present a new workflow to assess biogenic gas occurrences in continental shelf

716   settings at the basin scale where microbial CH_4 is sourced from recent continental-derived OM. This

717   new approach, applied and calibrated to the offshore Aquitaine, can help estimate the total CH_4

718   emitted naturally from shallow-water shelf areas that may reach the atmosphere. This subject is of

719   particular interest for the scientific community working on the impact of global warming issues as

720   methane is a major greenhouse gas with a negative contribution on climate and environment.

8. Acknowledgments

9. References

IPCC (2013). Climate Change 2013: The Physical Science Basis. Contribution of Working Group I to the Fifth Assessment Report of the Intergovernmental Panel on Climate Change. Cambridge, UK and New York: Cambridge University Press. doi:10.1017/CBO9781107415324

ISO 12213-2 (2006) Natural gas - Calculation of compression factor - Part 2: Calculation using molar-composition analysis

Arndt, S.; Jørgensen, B.B.; LaRowe, D.E.; Middelburg, J.J. Pancost, R.D. Regnier, P. (2013). Quantifying the degradation of organic matter in marine sediments. A review and synthesis. *Earth-Science Reviews,* 123, 53–86. https://DOI: 10.1016/j.earscirev.2013.02.008.

Arning, E.T., van Berk, W., dos Santos Neto, E.V., Naumann, R., and Schulz, H.M. (2013). The quantification of methane formation in Amazon fan sediments (ODP leg 155, site 938) by hydrogeochemical modeling solid–aqueous solution–gas interactions. *Journal of South American Earth Sciences*, *42*, 205-215.

Artemieva, I.M.; Thybo, H. (2013): EUNAseis. A seismic model for Moho and crustal structure in Europe, Greenland, and the North Atlantic region. In: *Tectonophysics,* 609, pp. 97–153. DOI: 10.1016/j.tecto.2013.08.004.

Baudin, F.; Disnar, J.R.; Aboussou, A.; Savignac, F. (2015): Guidelines for Rock–Eval analysis of recent marine sediments. In: *Organic Geochemistry,* 86, pp. 71–80. DOI: 10.1016/j.orggeochem.2015.06.009.

Behar, F. Vandenbroucke, M. Tang, Y. Marquis, F. and Espitalié, J. 1997, Thermal cracking of kerogen in open and closed systems: determination of kinetic parameters and stoichiometric coefficients for oil and gas generation. Organic Geochemistry, 26, 321–339

Behar, F.; Beaumont, V.; B. Penteado, H.L.D.B. (2001): Rock-Eval 6 Technology. Performances and Developments. In: *Oil and Gas Science and Technology - Rev. IFP* n. 2, 56, pp. 111–134. DOI: 10.2516/ogst:2001013.

Belyaev, S.S.; Wolkin, R.; Kenealy, W.R.; De Niro, M.J.; Epstein S.; Zeikus, J.G. (1983): Methanogenic Bacteria from the Bondyuzhskoe Oil Field: General Characterization and Analysis of Stable-Carbon Isotopic Fractionation. In: *Applied and Environmental Microbiology* n. 2, 45, pp. 691–697.

760 Biteau, J.J.; Le Marrec, A.; Le Vot, M.; Masset, J.M. (2006): The Aquitaine Basin. In: *Petroleum*
761 *Geoscience* n. 12, pp. 247–273.

762 Boetius, A.; Ravenschlag, K.; Schubert, C.J.; Rickert, D.; Widdel, F.; Gieseke, A. et al. (2000): A
763 marine microbial consortium apparently mediating anaerobic oxidation of methane. In: *Nature* n.
764 6804, 407, pp. 623–626. DOI: 10.1038/35036572.

765 Boillot, G.; Dupeuble, P.A.; Malod, J. (1979): Subduction and tectonics on the continental margin off
766 northern Spain. In: *Marine Geology* n. 1-2, 32, pp. 53–70. DOI: 10.1016/0025-3227(79)90146-4.

767 Bois, C.; Pinet, B.; Gariel, O. (1997): The sedimentary cover along the ECORS Bay of Biscay deep
768 seismic reflection profile. A comparison between the Parentis basin and other European rifts and
769 basins. In: *Mémoires de la Société géologique de France*, n. 171, pp. 143–165.

770 Boudreau, B.P. and Ruddick, B.R. (1991): On a reactive continuum representation of organic matter
771 diagenesis. In: *American Journal of Science* n. 5, 291, pp. 507–538. DOI: 10.2475/ajs.291.5.507.

772 Brothers, D.S. Ruppel, C. Kluesner, J.W. Ten Brink, U.S. Chaytor, J.D. Hill, J. C. Andrews, B.D and
773 Flores, C. (2014). Seabed fluid expulsion along the upper slope and outer shelf of the US Atlantic
774 continental margin. Geophysical Research Letters, 41(1), 96-101.

775 Bruneau, B. Villié, M. Ducros, M. Chauveau, B. Baudin, F. and Moretti, I. (2018). 3D Numerical
776 Modelling and Sensitivity Analysis of the Processes Controlling Organic Matter Distribution and
777 Heterogeneity—A Case Study from the Toarcian of the Paris Basin. Geosciences, 8(11), 405.

778 Brunet, M.F. (1994): Subsidence in the Parentis Basin (Aquitaine, France): Implications of the
779 Thermal Evolution. In: *Hydrocarbon and Petroleum Geology of France*. Volume 4 ISBN : 978-3-642-
780 78851-2

781 Brunet, M-F (1997): Subsidence along the ECORS Bay of Biscay deep seismic profile. In: *Mémoires*
782 *de la Société géologique de France,* 171, pp. 167–176.

783 Burdige, D.J. (2007): Preservation of organic matter in marine sediments: controls, mechanisms, and
784 an imbalance in sediment organic carbon budgets? In: *Chemical reviews* n. 2, 107, pp. 467–485. DOI:
785 10.1021/cr050347q.

786 Burdige, D.J. (2011): Temperature dependence of organic matter remineralization in deeply-buried
787 marine sediments. In: *Earth and Planetary Science Letters* n. 3-4, 311, pp. 396–410. DOI:
788 10.1016/j.epsl.2011.09.043.

789 Canuel, E.A. and Martens, C.S. (1996). Reactivity of recently deposited organic matter: Degradation
790 of lipid compounds near the sediment-water interface. Geochimica et cosmochimica acta, 60 (10),
791 1793-1806.

792 Carr, A.D. (2000): Suppression and retardation of vitrinite reflectance, Part 1. Formation and
793 significance for hydrocarbon generation. In: *Journal of Petroleum Geology* n. 23, pp. 313–343.

794 Clayton, C. (1992): Source Volumetrics of Biogenic Gas Generation. In: *Bacterial Gas*, 1992, pp.
795 191–204.

796 Cohen, D., Person, M., Wang, P., Gable, C.W., Hutchinson, D., Marksamer, A., Dugan B., Kooi, K.,
797 Groen, K., Lizarralde, D., Evan,s R.L., Day☐Lewis, F.D., Lane, J.W.J. (2010). Origin and extent of
798 fresh paleowaters on the Atlantic continental shelf, USA. Ground Water, 48(1), 143-158.

799 Conrad, R. (2005). Quantification of methanogenic pathways using stable carbon signatures: a review
800 and a proposal. Org. Geochem. 36, 739-572.

801 Cowie, G. L., Hedges, J. I., & Calvert, S. E. (1992). Sources and relative reactivities of amino acids,
802 neutral sugars, and lignin in an intermittently anoxic marine environment. *Geochimica et*
803 *Cosmochimica Acta*, *56*(5), 1963-1978.

804 Cremer, M. (1983). Approches sédimentologique et géophysique des accumulations turbiditiques:
805 l'éventail profond du Cap Ferret (Golfe de Gascogne), la série des grès d'Annot (Alpes de Haute
806 Provence). Thèse de doctorat de l'Université Bordeaux 1, 419 pp.

807 Dembicki, H. (2016): Practical petroleum geochemistry for exploration and production. 1st edition.
808 Waltham MA: Elsevier.

809 Deming, D. (1989): Application of bottom-hole temperature corrections in geothermal studies. In:
810 *Geothermics* n. 5-6, 18, pp. 775–786. DOI: 10.1016/0375-6505(89)90106-5.

811 Desegaulx, P.; Brunet, M.F. (1990): Tectonic subsidence of the Aquitaine Basin since Cretaceous
812 times. In: *Bulletin de la Société Géologique de France* n. 2, VI, pp. 295–306. DOI:
813 10.2113/gssgfbull.VI.2.295.

814 Dickens, G.R. (2004): Hydrocarbon-driven warming. In: *Nature* n. 429, 6991, pp. 513–515.

815 Dieckmann, V. (2005): Modelling petroleum formation from heterogeneous source rocks: the
816 influence of frequency factors on activation energy distribution and geological prediction. Marine and
817 Petroleum Geology, 22, 375-390.

818 Duan, Z.; Moller, N.; Weare, J.H. (1992). Prediction of methane solubilities in natural waters to high
819 ionic strength from 0 to 250 _C and from 0 to 1600 bar. Geochim.Cosmochim. Acta 56, 1451–1460.

820 Ducros, M. and Wolf, S. (2014): Tests des développements du modèle de génération du gaz
821 biogénique dans Visco. IFPEN Internal Report (R161/MD-OC 14-005).

822 Ducros, M.; Cacas, M.C.; Rouchon, V.; Wolf, S.; Blanchet, D.; Ravin, A.; Pujol, A. (2015):
823 Simulation of anaerobic SOM biodegradation and biogenic methane production in the TemiFlow basin
824 model. IMOG. Prague, 2015.

825 Dudley D.R. and George E.C. (1981): Generation, Accumulation, and Resource Potential of Biogenic
826 Gas. In: *AAPG Bulletin* n. 1, 65, pp. 5–25.

827 Dupré, S. (2013) GAZCOGNE2 cruise, RV Pourquoi pas ? doi:https://doi.org/10.17600/13030090

828 Dupré, S. Woodside, J. Foucher, J.P. de Lange, G. Mascle, J. Boetius, A. Mastalerz, V. Stadnitskaia,
829 A. Ondréas, H. Huguen, C. Harmegnies, F. Gontharet, S. Loncke, L. Deville, E. Niemann, H.
830 Omoregie, E. Olu-Le Roy, K. Fiala-Medioni, A. Dählmann, A. Caprais, J.C. Prinzhofer, A. Sibuet, M.
831 Pierre, C. Sinninghe Damsté, J. NAUTINIL scientific Party (2007) Seafloor geological studies above
832 active gas chimneys off Egypt (Central Nile Deep Sea Fan). Deep Sea Research Part I: Oceanographic
833 Research Papers 54 (7):1146-1172. doi:10.1016/j.dsr.2007.03.007

834 Dupré, S.; Berger, L.; Le Bouffant, N.; Scalabrin, C.; Bourillet, J.F. (2014): Fluid emissions at the
835 Aquitaine Shelf (Bay of Biscay, France). A biogenic origin or the expression of hydrocarbon leakage?
836 In: *Continental Shelf Research,* 88, pp. 24–33. DOI: 10.1016/j.csr.2014.07.004.

837 Dupré, S. Loubrieu, B. Pierre, C. Scalabrin, C. Guérin, C. Ehrhold, A. Ogor, A. Gautier, E. Ruffine, L.
838 Biville, R. Saout, J. Breton, C. Floodpage, J. Lescanne, M. (2020) The Aquitaine Shelf Edge (Bay of
839 Biscay): A Primary Outlet for Microbial Methane Release. Geophysical Research Letters 47
840 (7):e2019GL084561. doi:10.1029/2019gl084561.

841 Espitalié, J.; Deroo, G.; Marquis, F. (1985): Rock-Eval pyrolysis and its applications. In: *Revue De*
842 *Institut Francais Du Petrole* n. 5, 40, pp. 563–579.

843 Espitalié, J.; Madec, M.; Tissot, B.; Mennig, J. J.; Leplat, P. (1977): Source Rock Characterization
844 Method for Petroleum Exploration. In:. Offshore Technology Conference. OTC, 1977/1/1: Offshore
845 Technology Conference, p. 6.

846 Etiope, G. and Klusman, R. W. (2002). Geologic emissions of methane to the atmosphere.
847 *Chemosphere*, *49*(8), 777-789.

848 Etiope, G. Lassey, K.R. Klusman, R.W. and Boschi, E. (2008). Reappraisal of the fossil methane
849 budget and related emission from geologic sources. Geophysical Research Letters, 35(9).

850 Etiope, G. and Klusman, R. W. (2010). Methane microseepage in drylands: soil is not always a CH_4
851 sink. Journal of Integrative Environmental Sciences, 7(S1), 31-38.

852 Etiope, G. and Schwietzke, S. (2019). Global geological methane emissions: an update of top-down
853 and bottom-up estimates. Elementa-Science of the Anthropocene.

854 Ferrer, O.; Roca, E.; Benjumea, B.; Muñoz, J. A.; Ellouz, N.; MARCONI Team (2008): The deep
855 seismic reflection MARCONI-3 profile. Role of extensional Mesozoic structure during the Pyrenean
856 contractional deformation at the eastern part of the Bay of Biscay. In: *Marine and Petroleum Geology*
857 n. 8, 25, pp. 714–730. DOI: 10.1016/j.marpetgeo.2008.06.002.

858 Floodgate, G.D.; Judd, A.G. (1992): The origins of shallow gas. In: *Continental Shelf Research* n. 10,
859 12, pp. 1145–1156. DOI: 10.1016/0278-4343(92)90075-U.

860 Fujii, T., Tin Aung, T., Wada, N., Komatsu, Y., Suzuki, K., Ukita, T., Wygrala, B., Fuchs, T., Rottke,
861 W., Egawa, K. (2016). Modeling gas hydrate petroleum systems of the Pleistocene turbiditic
862 sedimentary sequences of the Daini-Atsumi area, eastern Nankai Trough, Japan. *Interpretation*, *4*(1),
863 SA95-SA111.

864 Gervais, V.; Ducros, M.; and Granjeon, D. (2018). Probability maps of reservoir presence and
865 sensitivity analysis in stratigraphic forward modeling. AAPG Bulletin, 102(4), 613-628.

866 Hedges, J. I., and Oades, J. M. (1997). Comparative organic geochemistries of soils and marine
867 sediments. *Organic geochemistry*, *27*(7-8), 319-361.

868 Homma, T. and Saltelli, A. (1996): Importance measures in global sensitivity analysis of model
869 output: Reliability Engineering and System Safety, v. 52, no. 1, p. 1–17, doi: 10.1016/0951-
870 8320(96)00002-6.

871 Hornafius, J.S.; Quigley, D.; and Luyendyk, B.P. (1999). The world's most spectacular marine
872 hydrocarbon seeps (Coal Oil Point, Santa Barbara Channel, California): Quantification of emissions.
873 Journal of Geophysical Research: Oceans, 104(C9), pp. 20703-20711.

874 Hovland, M.; Judd, A.G.; Burke, R.A. (1993) The global production of methane from shallow
875 submarine sources. Chemosphere, 26,559–78

876 Hovland, M.; Gardner, J.V.; Judd, A.G. (2002): The significance of pockmarks to understanding fluid
877 flow processes and geohazards. In: *Geofluids* n. 2, 2, pp. 127–136. DOI: 10.1046/j.1468-
878 8123.2002.00028.x.

879 Janssen, B.H. (1984): A simple method for calculating decomposition and accumulation of 'young' soil
880 organic matter. In: *Plant and Soil,* 76, pp. 297–304.

881 Jensen, P. (1992): "Bubbling reefs' in the Kattegat: submarine landscapes of carbonate- cemented
882 rocks support a diverse ecosystem at methane seeps. In: *Mar. Ecol. Prog. Ser* n. 83, pp. 103–112.

883 Jones, R.W. Edison, A. (1979): Microscopic observations of kerogen related to geochemical
884 parameters with emphasis on thermal maturation. In: *Society Economic Paleontologists and*
885 *Mineralogists*, pp. 1–12.

886 Johnson, H.P. Miller, U.K. Salmi, M.S. and Solomon, E.A. (2015). Analysis of bubble plume
887 distributions to evaluate methane hydrate decomposition on the continental slope. Geochemistry,
888 Geophysics, Geosystems, 16(11), pp. 3825-3839.

889 Judd, A.G. Davies, G. Wilson, J. Holmes, R. Baron, G. Bryden, I. (1997). Contributions to
890 atmospheric methane by natural seepages on the UK continental shelf. Marine Geology, 137, 427–55.

891 Judd, A.G.; Hovland, M.; Dimitrov, L.I.; Garcia Gil, S.; Jukes, V. (2002): The geological methane
892 budget at Continental Margins and its influence on climate change. In: *Geofluids* n. 2, 2, pp. 109–126.
893 DOI: 10.1046/j.1468-8123.2002.00027.x.

894 Judd, A.G. (2004). Natural seabed gas seeps as sources of atmospheric methane. Environmental
895 Geology, 46(8), 988-996.

896 Kamga, N. (2016). "Low-Temperature Artificial Maturation Studies of Type II and Type III Kerogens:
897 Implications for Biogenic Gas Production". Doctor of Philosophy (PhD), Dissertation, Chemistry and
898 Biochemistry, Old Dominion University, DOI: 10.25777/5sj5-4y45.

899 Katz, B.J. (2011): Microbial Processes and Natural Gas Accumulations. In: *TOGEOJ* n. 1, 5, pp. 75–
900 83. DOI: 10.2174/1874262901105010075.

901 Khalil, M.A.K. (2013). Atmospheric methane: sources, sinks, and role in global change (Vol. 13).
902 Springer Science and Business Media.

903 Klusman, R.W.; Leopold, M.E.; LeRoy, M.P. (2000). Seasonal variation in methane fluxes from
904 sedimentary basins to the atmosphere: Results from chamber measurements and modeling of transport
905 from deep sources. Journal of Geophysical Research: Atmospheres, 105(D20), 24661-24670.

906 Kvenvolden, K.A. (1993): Gas hydrates geological perspective and global change. In: *American
907 Geophysical Union*, pp. 173–187.

908 Kvenvolden, K.A.; Lorenson, T.D.; Reeburgh, W.S. (2001). Attention turns to naturally occurring
909 methane seepage. Eos, Transactions American Geophysical Union, 82(40), 457-457.

910 Lafargue, E.; Marquis, F.; Pillot, D. (1998): Rock-Eval 6 Applications in Hydrocarbon Exploration,
911 Production, and Soil Contamination Studies. In: *Rev. Inst. Fr. Pét.* n. 4, 53, pp. 421–437. DOI:
912 10.2516/ogst:1998036.

913 Lash, G.G. (2015). Pyritization induced by anaerobic oxidation of methane (AOM)–An example from
914 the upper devonian shale succession, western New York, USA. Marine and Petroleum Geology, 68,
915 520-535. https://doi.org/10.1016/j.marpetgeo.2015.10.002.

916 Lazure, P.; Jégou, A.M.; Kerdreux, M. (2006): Analysis of salinity measurements near islands on the
917 French continental shelf of the Bay of Biscay. In: *Scientia Marina*, 70, p.7-14, DOI:
918 10.3989/scimar.2006.70s17

919 Loubrieu, B. (2013) GAZCOGNE1 cruise, RV Le Suroît. doi:https://doi.org/10.17600/13020070

920 McKay, M.D.; Beckman, R.J.; Conover, W.J. (1979): Comparison of three methods for selecting
921 values of input variables in the analysis of output from a computer code: Technometrics, v. 21, no. 2,
922 p. 239–245.
923

924 McKenzie, D. (1978): Some remarks on the development of sedimentary basins. In: *Earth and*
925 *Planetary Science Letters* n. 1, 40, pp. 25–32. DOI: 10.1016/0012-821X(78)90071-7.

926 McTavish, R.A. (1978): Pressure retardation of vitrinite diagenesis, offshore north-west Europe. In:
927 *Nature* n. 271, pp. 648–650.

928 Michel, G.; Dupré, S.; Baltzer, A.; Ehrhold, A.; Imbert, P.; Pitel, M. et al. (2017): Pockmarks on the
929 South Aquitaine Margin continental slope: the 2 seabed expression of past fluid circulation and bottom
930 currents Corresponding Author. In: *Comptes Rendus Géoscience, Elsevier Masson* n. 8, 349, pp. 391–
931 401.

932 Michel G. (2017) Mise en place et pérennisation d'un vaste système fluide microbien sur le Plateau
933 Aquitain: caractérisation et facteurs de contrôle. Thèse de doctorat de l'Université Pierre et Marie
934 Curie, Paris, pp. 482.

935 Middelburg, J.J. (1989): A simple rate model for organic matter decomposition in marine sediments.
936 In: *Geochimica et Cosmochimica Acta* n. 7, 53, pp. 1577–1581. DOI: 10.1016/0016-7037(89)90239-1.

937 Middelburg, J.J.; Klaver, G.; Nieuwenhuize, J.; Wielemaker, A.; de Haas, W.; Vlug, T.; van der Nat,
938 J.F. (1996). Organic matter mineralization in intertidal sediments along an estuarine gradient. Marine
939 Ecology Progress Series, 132, 157-168.

940 Mitterer, R.M. (2010). Methanogenesis and sulfate reduction in marine sediments: A new
941 model. *Earth and Planetary Science Letters*, *295*(3-4), 358-366.

942 Oberlin, A.; Boulmier, J.L.; Villey, M. (1980). Electron microscopic study of kerogen microtexture.
943 In: Durand, B. (Ed.), Selected Criteria for Determining the Evolution Path and Evolution Stage of
944 Kerogen. Kerogen, Editions Technip, Paris, pp. 191–242.

945 Ortiz, A.; Guillocheau, F.; Lasseur, E.; Briais, J.; Robin, C.; Serrano, O.; Fillon, C. (2020). Sediment
946 routing system and sink preservation during the post-orogenic evolution of a retro-foreland basin: The
947 case example of the North Pyrenean (Aquitaine, Bay of Biscay) Basins. Marine and Petroleum
948 Geology, vol. 112, p. 104085.

949 Pasquale, V.; Gola, G.; Chiozzi, P.; Verdoya, M. (2011): Thermophysical properties of the Po Basin
950 rocks. In: *Geophysical Journal International* n. 1, 186, pp. 69–81. DOI: 10.1111/j.1365-
951 246X.2011.05040.x.

952 Paull, C.K., and Ussler III, W. (2008, July). Re-evaluating the significance of seafloor accumulations
953 of methane-derived carbonates: seepage or erosion indicators. In *Proceedings of the 6th International*
954 *Conference on Gas Hydrates (ICGH 2008), Vancouver, British Columbia, Canada, July* (pp. 6-10).

955 Peters, K.E.; Burnham, A.K.; Walters, C.C.; Schenk, O. (2018). Guidelines for kinetic input to
956 petroleum system models from open-system pyrolysis. Marine and Petroleum Geology, 92, 979-986.

957 Pierre, C.; Demange, J.; Blanc-Valleron, M.M.; Dupré, S. (2017a): Authigenic carbonate mounds from
958 active methane seeps on the southern Aquitaine Shelf (Bay of Biscay, France). Evidence for anaerobic
959 oxidation of biogenic methane and submarine groundwater discharge during formation. In:
960 *Continental Shelf Research,* 133, pp. 13–25. DOI: 10.1016/j.csr.2016.12.003.

961 Pierre C, Blanc-Valleron M-M, Boudouma O, Lofi J (2017b) Carbonate and silicate cementation of
962 siliciclastic sediments of the New Jersey shelf (IODP Expedition 313): relation with organic matter
963 diagenesis and submarine groundwater discharge. Geo-Marine Letters 37 (6):537-547.
964 doi:10.1007/s00367-017-0506-6

965 Pillot, D.; Deville, E.; Prinzhofer, A. (2014): Identification and Quantification of Carbonate Species
966 Using Rock-Eval Pyrolysis. In: *Oil Gas Sci. Technol. – Rev. IFP Energies nouvelles* n. 2, 69, pp. 341–
967 349. DOI: 10.2516/ogst/2012036.

968 Pujol, A.; Rouchon, V.; Ravin, A.; Wolf, S.; Blanchet, D.; Ducros, M.; Maurand, N. (2016):
969 Simulation of Anaerobic SOM Biodegradation and Biogenic Methane Production for Basin Modeling.
970 AAPG Hedberg Conference. Santa Barbara, California, 2016.

971 Reeburgh, W.S. (2007). Oceanic methane biogeochemistry. Chem. Rev. 107, 486-513.

972 Regnier, P. Dale, A.W. Arndt, S. La Rowe, D.E. Mogollon, J. Van Cappellen, P. (2011). Quantitative
973 analysis of anaerobic oxidation of methane (AOM) in marine sediments: a modeling perspective.
974 Earth-Sci. Rev. 106, pp. 105-130.

975 Rice, D.D. (1992): Controls, habitat, and resource potential of ancient bacterial gas. In: *Bacterial Gas*,
976 1992, pp. 91–118.

977 Rice, D.D. and Claypool, G.E. (1981): Generation, Accumulation, and Resource Potential of Biogenic
978 Gas. In: *AAPG Bulletin* n. 1, 65, pp. 5–25.

979 Robinson, A.R. and Brink, K.H. (2005). The global coastal ocean: multiscale interdisciplinary
980 processes (Vol. 13). Harvard University Press.

981 Roca, E.; Muñoz, J.A.; Ferrer, O.; Ellouz, N. (2011): The role of the Bay of Biscay Mesozoic
982 extensional structure in the configuration of the Pyrenean orogen. Constraints from the MARCONI
983 deep seismic reflection survey. In: *Tectonics* n. 2, 30, n/a-n/a. DOI: 10.1029/2010TC002735.

984 Römer, M.; Sahling, H.; Pape, T.; Bahr, A.; Feseker, T.; Wintersteller, P.; Bohrmann, G. (2012):
985 Geological control and magnitude of methane ebullition from a high-flux seep area in the Black Sea—
986 the Kerch seep area. In: *Marine Geology,* 319-322, pp. 57–74. DOI: 10.1016/j.margeo.2012.07.005.

987 Ruffine, L.; Donval, J.P.; Croguennec, C.; Bignon, L.; Birot, D.; Battani, A. Bayon, G.; Caprais, J.C.;
988 Lantéri, N.; Levaché, D.; Dupré, S. (2017): Gas Seepage along the Edge of the Aquitaine Shelf
989 (France). Origin and Local Fluxes. In: *Geofluids* n. 66, 2017, pp. 1–13. DOI: 10.1155/2017/4240818.

990 Saunois, M.; Bousquet, P.; Poulter, B.; Peregon, A.; Ciais, P.; Canadell, J. G.; ... and Janssens-
991 Maenhout, G. (2016). The global methane budget 2000–2012. Earth System Science Data, 8(2), 697-
992 751.

993 Schenk, H.J.; Horsfield, B.; Krooss, B.; Schaefer, R.G.; Schwochau, K. (1997)b. Kinetics of petroleum
994 formation and cracking, Petroleum and basin evolution; insights from petroleum geochemistry,
995 geology and basin modeling. Springer, Berlin, Federal Republic of Germany

996 Schneider, F.; Dubille M.; Montadert, L. (2016) Modeling of microbial gas generation: application to
997 the eastern Mediterranean "Biogenic Play". Geologica Acta 14 (4), pp. 403-417.
998 doi:10.1344/GeologicaActa2016.14.4.5

999 Schulz, H.D. and Zabel, M. (2006): Marine geochemistry. 2nd rev. updated and extended ed. Berlin,
1000 New York: Springer.

1001 Schwietzke, S.; Sherwood, O.A.; Bruhwiler, L.M.; Miller, J.B.; Etiope, G.; Dlugokencky, E.J.; ... and
1002 Tans, P.P. (2016). Upward revision of global fossil fuel methane emissions based on isotope database.
1003 Nature, 538(7623), 88-91.

1004 Sibuet, J.C.; Monti, S.; Loubrieu, B.; Mazé, J.P.; Srivastava, S. (2004). Carte bathymétrique de
1005 l'Atlantique nord-est et du golfe de Gascogne: implications cinématiques (9 fig. 1 pl ht). *Bulletin-
1006 Societe Geologique De France*, 175, 429-442.

29

1007 Skarke, A.; Ruppel, C.; Kodis, M.; Brothers, D.; Lobecker, E. (2014): Widespread methane leakage
1008 from the sea floor on the northern US Atlantic margin. In: *Nature Geosci* n. 9, 7, pp. 657–661. DOI:
1009 10.1038/ngeo2232.

1010 Sobol', I.M. 1990, On sensitivity estimation for nonlinear mathematical models: Mathematical
1011 Modeling and Computational Experiment, v. 1, no. 4, p. 407–414.

1012 Snyder, G.T.; Dickens, G.R.; Tomaru, H.; Takeuchi, R.; Komatsubara, J.; Ishida, Y.; Yu, H. (2007)
1013 Pore water profiles and authigenic mineralization in shallow marine sediments above the methane-
1014 charged system on Umitaka Spur, Japan sea. Deep-sea Research, part II. Top. Stud. Oceanogr. 54,
1015 1216-1239.

1016 Starling, K.E. and Savidge, J.L. (1992). Compressibility factors of natural gas and other related
1017 hydrocarbon gases. American Gas Association, Operating Section.

1018 Thauer, R.K. (2010). Functionalization of methane in anaerobic microorganisms. Angewandte Chemie
1019 International Edition, 49(38), 6712-6713.

1020 Thinon, I.; Fidalgo-González, L.; Réhault, J.P.; Olivet, J.L. (2001): Déformations pyrénéennes dans le
1021 golfe de Gascogne. In: *Comptes Rendus de l'Académie des Sciences - Series IIA - Earth and Planetary*
1022 *Science* n. 9, 332, pp. 561–568. DOI: 10.1016/S1251-8050(01)01576-2.

1023 Thomas, J.; Frost, R.R.; Harvey, R.D. (1973): Thermal conductivity of carbonate rocks. In:
1024 *Engineering Geology* n. 1, 7, pp. 3–12. DOI: 10.1016/0013-7952(73)90003-3.

1025 Toole, J.M. (1981): Sea ice, winter convection, and the temperature minimum layer in the Southern
1026 Ocean. In: *Journal of Geophysical Research: Oceans* n. C9, 86, pp. 8037–8047. DOI:
1027 10.1029/JC086iC09p08037.

1028 Tugend, J.; Manatschal, G.; Kusznir, N.J.; Masini, E. (2015): Characterizing and identifying structural
1029 domains at rifted continental margins. Application to the Bay of Biscay margins and its Western
1030 Pyrenean fossil remnants. In: *Geological Society, London, Special Publications* n. 1, 413, pp. 171–
1031 203. DOI: 10.1144/SP413.3.

1032 Tugend, J.; Manatschal, G.; Kusznir, N. J.; Masini, E.; Mohn, G.; Thinon, I. (2014): Formation and
1033 deformation of hyperextended rift systems. Insights from rift domain mapping in the Bay of Biscay-
1034 Pyrenees. In: *Tectonics* n. 7, 33, pp. 1239–1276. DOI: 10.1002/2014TC003529.

1035 van Hinsbergen, D.J.J.; de Groot, L.V.; van Schaik, S.J.; Spakman, W.; Bijl, P.K.; Sluijs, A.;
1036 Langereis, C.G.; Brinkhuis, H. (2015): A Paleolatitude Calculator for Paleoclimate Studies. PloS one
1037 (6).

1038 Vandenbroucke, M., and Largeau, C. (2007). Kerogen origin, evolution and structure. *Organic*
1039 *Geochemistry*, *38*(5), 719-833.

1040 Wallmann, K.; Aloisi, G.; Haeckel, M.; Obzhirov, A.; Pavlova, G.; Tishchenko, P. (2006): Kinetics of
1041 organic matter degradation, microbial methane generation, and gas hydrate formation in anoxic marine
1042 sediments. In: *Geochimica et Cosmochimica Acta* n. 15, 70, pp. 3905–3927. DOI:
1043 10.1016/j.gca.2006.06.003.

1044 Wellsbury, P., Mather, I., & Parkes, R. J. (2002). Geomicrobiology of deep, low organic carbon
1045 sediments in the Woodlark Basin, Pacific Ocean. *FEMS microbiology ecology*, *42*(1), 59-70.

1046 Wendebourg, J. (2003). Uncertainty of petroleum generation using methods of experimental design
1047 and response surface modeling: application to the Gippsland Basin, Australia. In: Düppenbecker, S.

1048 Marzi, R. (Eds.), Multidimensional Basin Modeling, AAPG/Datapages Discovery Series, vol. 7, pp.
1049 295–307.

1050 Westrich, J.T. and Berner, R.A. (1984): The role of sedimentary organic matter in bacterial sulfate
1051 reduction: The G model tested1. In: *American Society of Limnology and Oceanography*, pp. 236–249,

1052 Whiticar, M.J. (1994): Correlation of Natural Gases with Their Sources: Chapter 16: Part IV.
1053 Identification and Characterization.

1054 Whiticar, M.J.; Faber, E.; Schoell M. (1986): Biogenic methane formation in marine and freshwater
1055 environments: CO2 reduction vs. acetate fermentation - Isotope evidence. In: *Geochimica et*
1056 *Cosmochimica Acta,* 50, pp. 693–709.

1057 Whiticar, M.J. (1999): Carbon and hydrogen isotope systematics of bacterial formation and oxidation
1058 of methane. In: *Chemical Geology* n. 1-3, 161, pp. 291–314. DOI: 10.1016/S0009-2541(99)00092-3.

1059 Wygrala, B. (1989). Integrated study of an oil field in the southern Po basin, northern Italy (No. FZJ-
1060 2014-03033). Publikationen vor 2000.

1061 Zonneveld, K.A., Versteegh, G. J., Kasten, S., Eglinton, T.I., Emeis, K. C., Huguet, C., Koch, B.P., de
1062 Lange, G.J., de Leeuw, J.W., Middelburg, J.J., Mollenhauer, G., Prahl, F.G., Rethemeyer, J.,
1063 Wakeham, S.G. (2010). Selective preservation of organic matter in marine environments; processes
1064 and impact on the sedimentary record. *Biogeosciences*, *7*(2), pp. 483-511.

1065

1066

1067

1068

1069

1070

1071

1072

1073

1074

1075

1076 FIGURES:

31
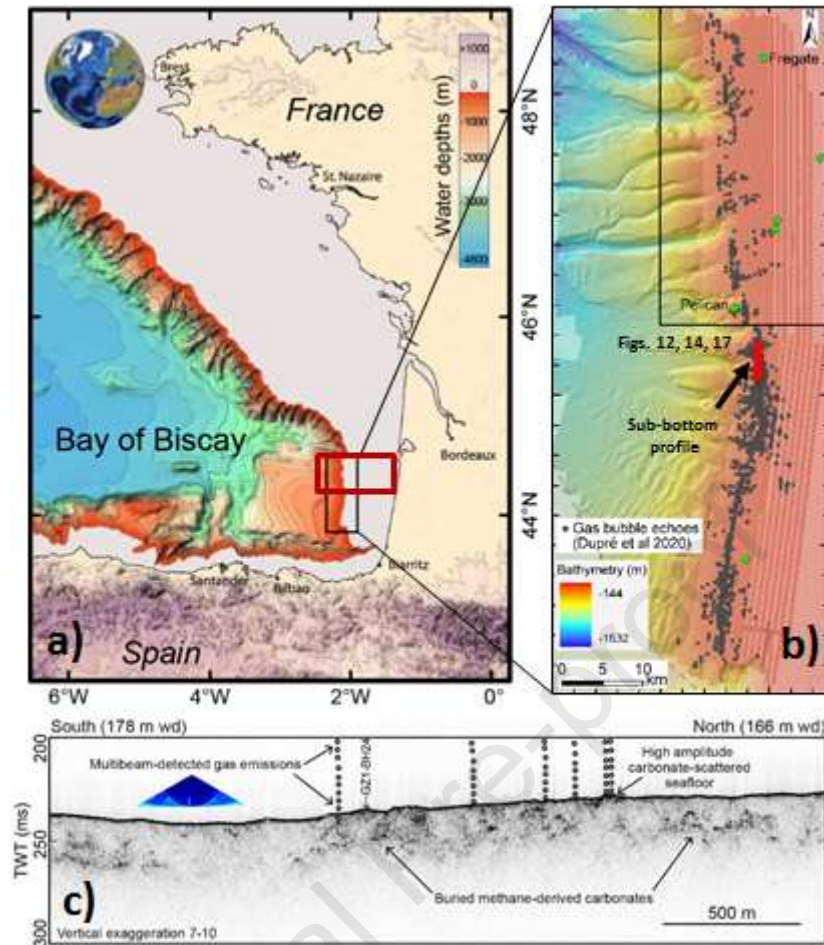
1077

Figure 1. a) Bathymetric map of the Bay of Biscay (Southwestern France) and modelled area (red rectangle) of Fig. 3 modified after Sibuet et al. (2004) and Dupré et al. (2020); b) Detailed shaded bathymetric map offshore Aquitaine (Loubrieu 2013, Gazcogne1) with gas emission site distribution and localization of the sub-bottom profile (red line) shown in Fig. 1c and the modelled offshore area in Fig. 1b (black rectangle) (modified after Dupré et al. 2020); c) Sub-bottom profile acquired in the emission site showing the presence of sub-cropping methane-derived authigenic carbonates from Dupré et al. (2020).

1084

1085

1086

1087
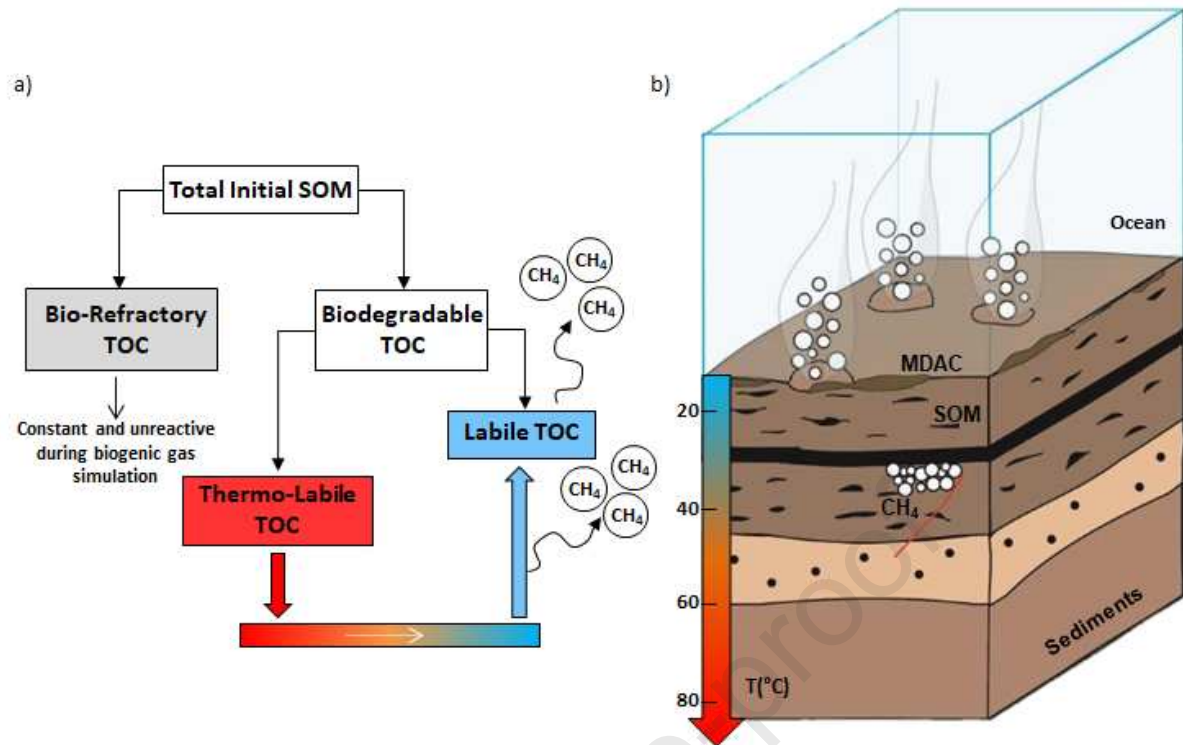
1088

Figure 2. a) Schematic diagram of the microbial gas generation concept. The gas is generated during the early diagenesis stage by the labile TOC. At greater burial and depth, the transformation of the thermo-labile TOC allows to produce new labile fraction that generate new gas. The bio-refractory TOC is non-reactive and constant during biogenic gas simulation but it can be transformed into hydrocarbons by thermogenic cracking at greater temperature (> 80°C). b) Schematic block diagram offshore Aquitaine.

1094

1095

1096

1097

1098

33
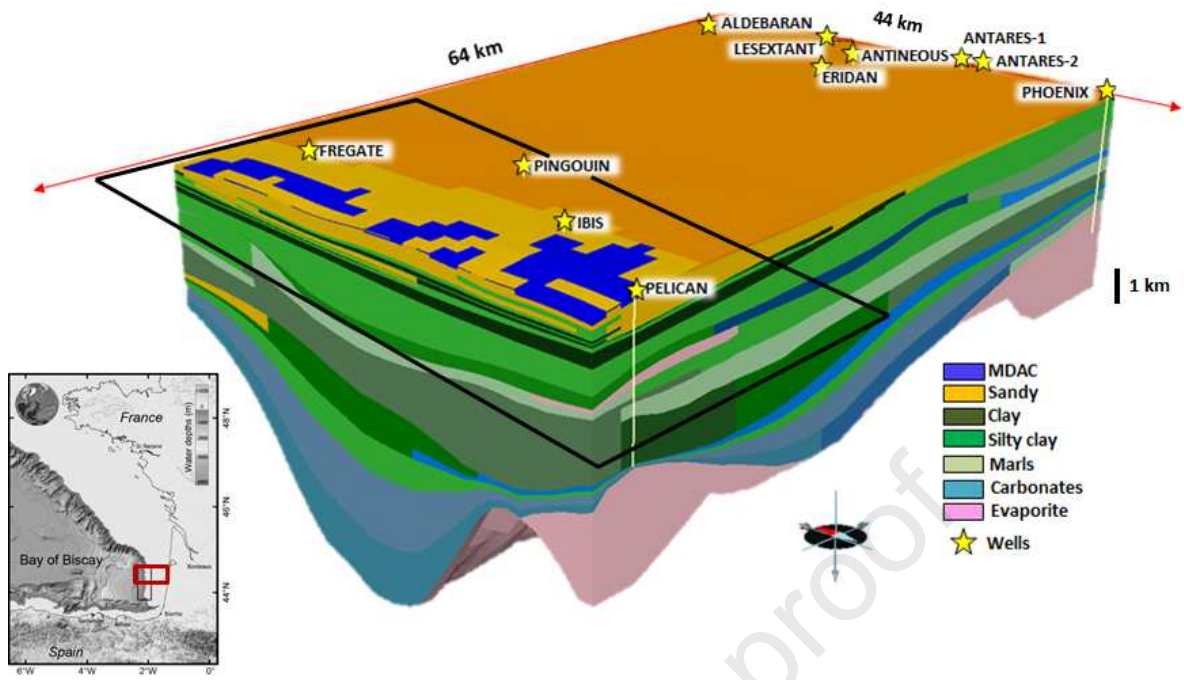
1099

1100 **Figure 3. 3D block diagram of the study area from TemisFlow®. The model covers an area of ~2800 km² representing**
1101 **a shelf part of the offshore Aquitaine Basin (red rectangle) (Fig. 1a) where seeps have been mapped (black rectangle)**
1102 **(Fig. 1b) with in situ measurements and annual estimation of methane flow rates (Dupré et al. 2020). The black**
1103 **rectangle represents the extent of maps in Figs. 12, 14 and 17.**

1104

1105

1106

1107

1108

1109

1110

1111

1112

1113

1114

1115

1116

1117

1118

1119

1120

1121

1122

1123
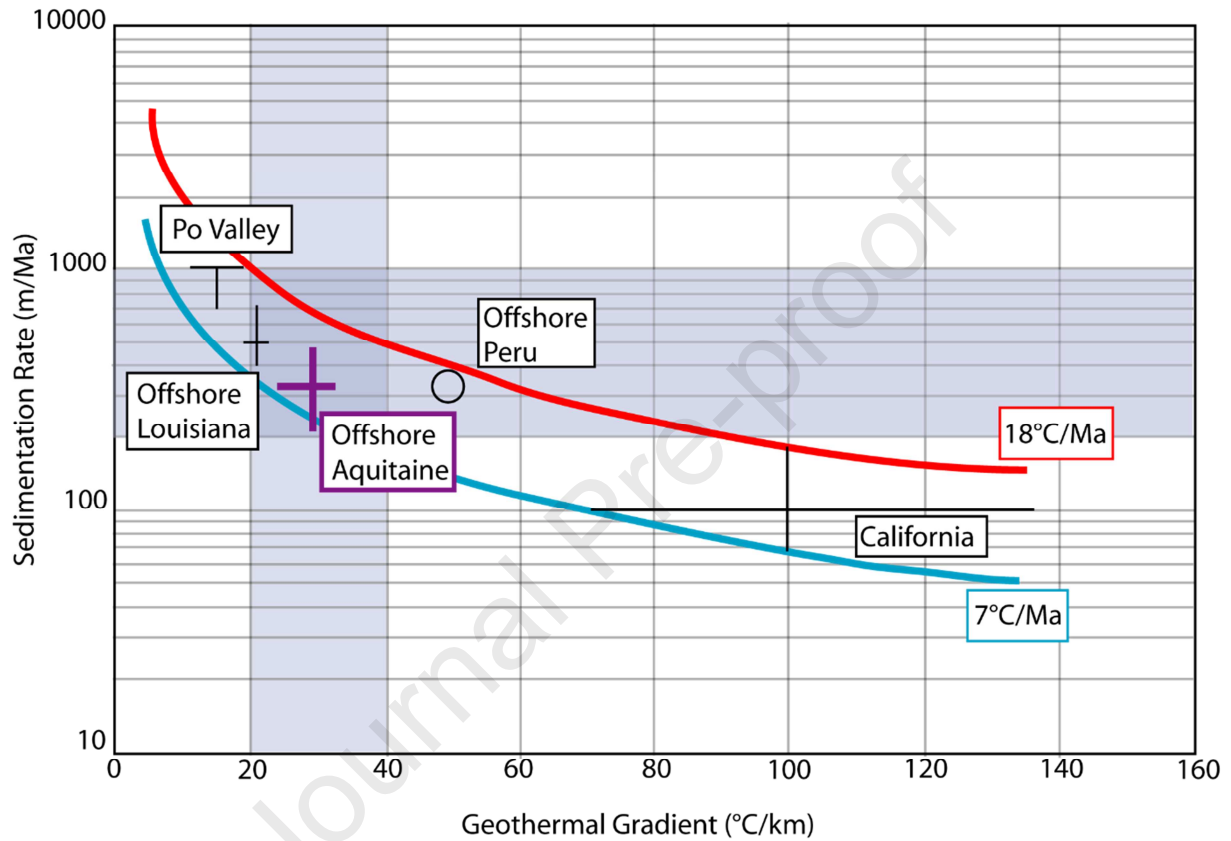
1124

1125 **Figure 4. Biogenic gas maturity windows based on the heating rate which is determined as a function of the**
1126 **sedimentation rate over the geothermal gradient (modified after Clayton 1992). The highlighted area indicates the**
1127 **normal geothermal gradient and sedimentation rate for worldwide sedimentary basins (Clayton 1992). In the offshore**
1128 **Aquitaine, the Plio-Pleistocene sequences are characterized by favorable conditions for biogenic gas generation**
1129 **(purple lines).**

1130

1131

1132

1133

1134

1135

1136

1137

1138
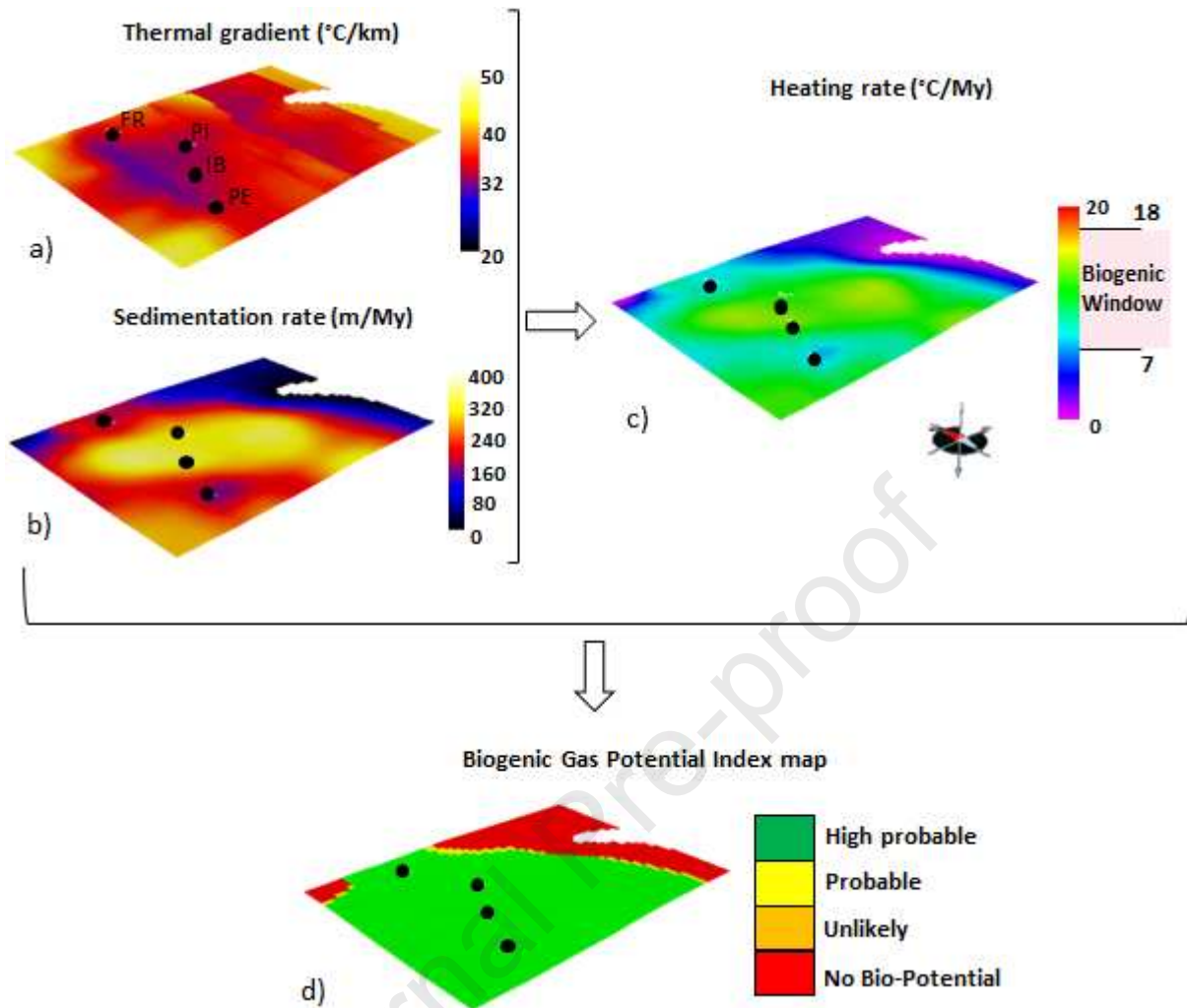
1139

Figure 5. The thermal gradient (a) and the sedimentation rate maps (b) computed in TemisFlow® are multiplied to obtain the heating rate map (c). This map is then converted into a "Biogenic Gas Potential Index" map (d) to determine the areas entering the biogenic maturity window in which any OM may be converted into microbial methane for the upper Miocene layer. Black dots represent offshore wells (FR – Fregate-1; PI – Pingouin-1; IB – Ibis-1; PE – Pelican-1) (for well locations see Fig. 3).

1145

1146

1147

1148

1149

1150

1151

1152

1153
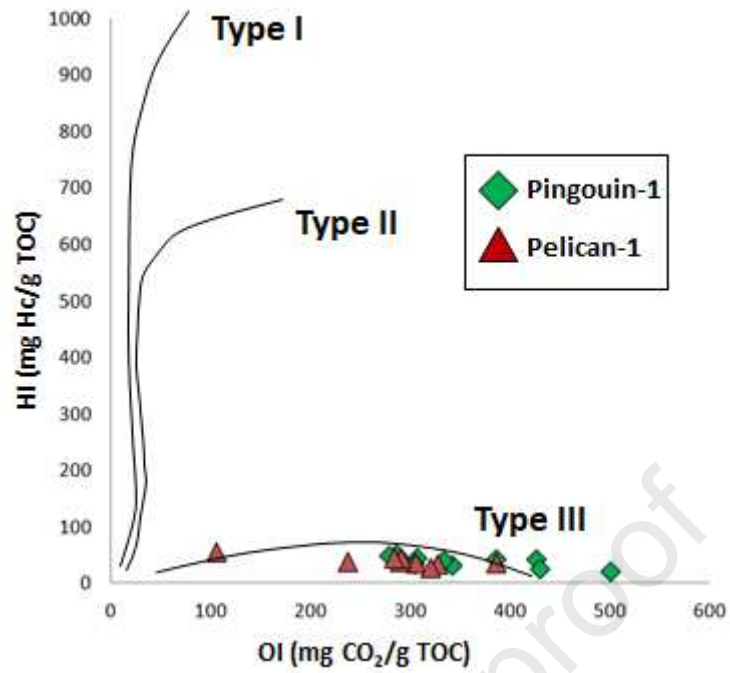
1154

Figure 6. Rock-Eval results on cuttings collected from Pelican-1 and Pingouin-1 wells offshore Aquitaine. Well locations are displayed in Figure 3. The OM derives from continental origin (Type III). The samples are mainly characterized by poor TOC content (see Table S1) and very low HI values.

1168
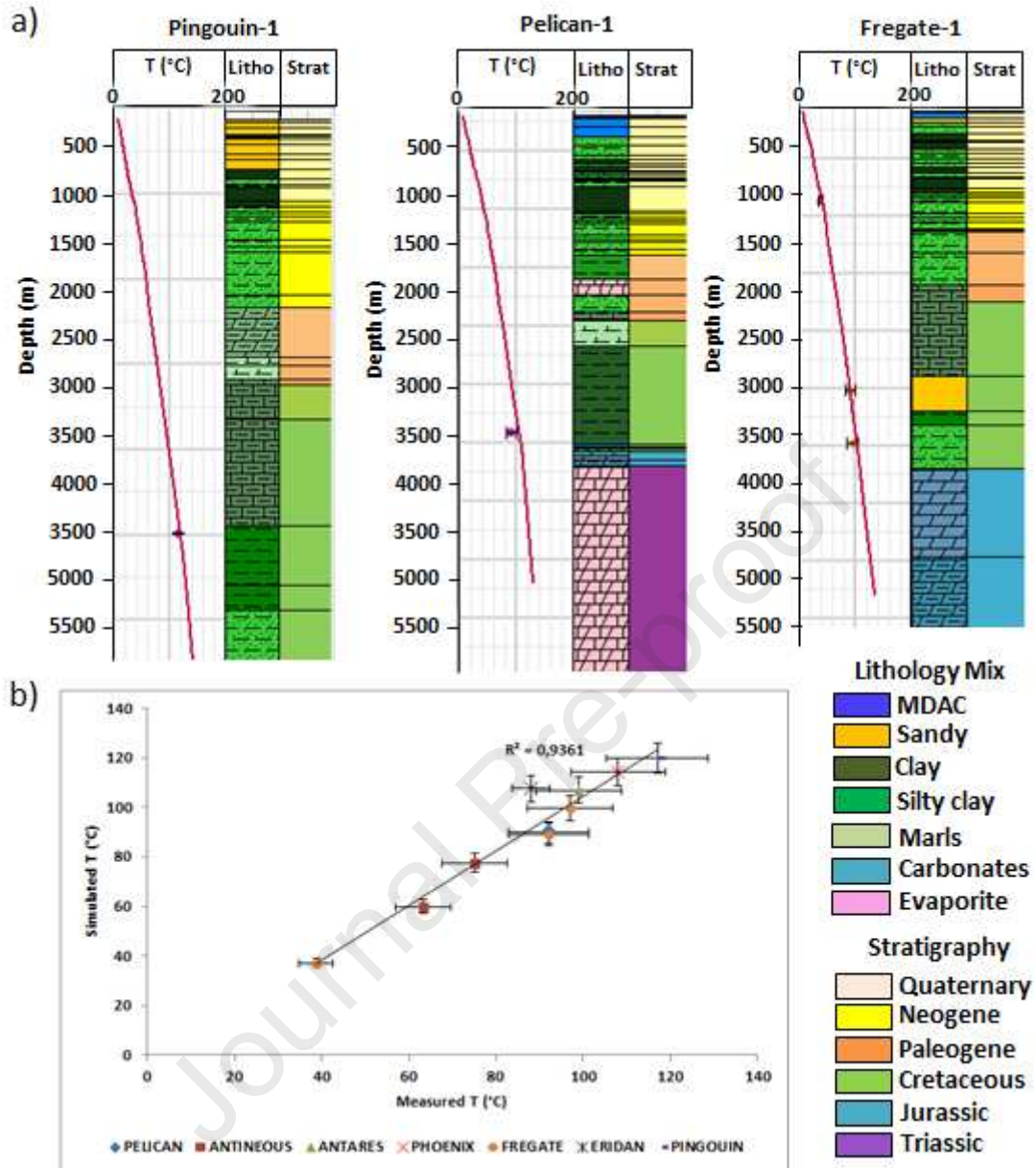
Figure 7. a) Present-day temperature calibration results for 3 wells located offshore Aquitaine with corresponding stratigraphy and lithology used in the 3D model. b) Temperature calibrations for all 7 wells are given by a cross-plot "Simulated vs Measured Temperatures". Well locations are shown in Figure 3.

1172

1173

1174

1175

1176

1177

1178

1179

1180

1181

1182

1183
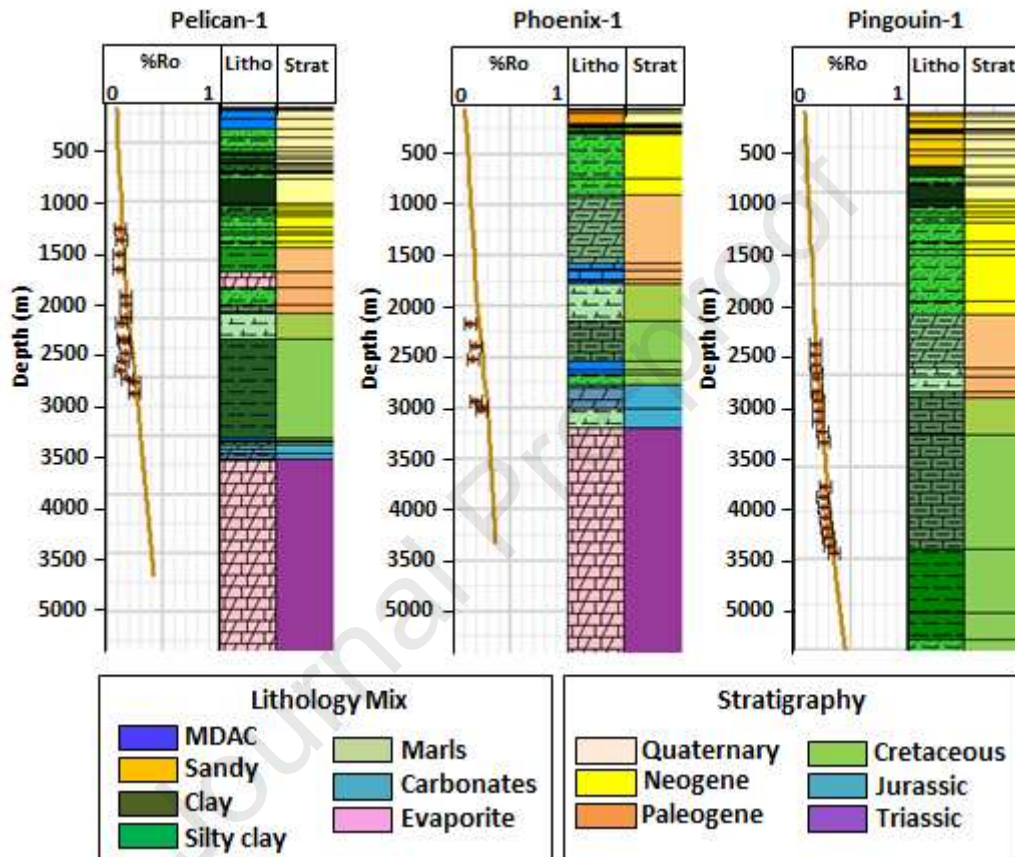
1184

Figure 8. Paleo-thermal calibration of vitrinite reflectance data for 3 of the 6 wells of the Aquitaine Basin with corresponding stratigraphy and lithology used in the model. The modelled maturities (orange curves) show a good fit with measured vitrinite reflectance values for all wells, staying within the standard deviation. Well locations are shown in Figure 3.

1189

1190

1191

1192

1193

1194

1195
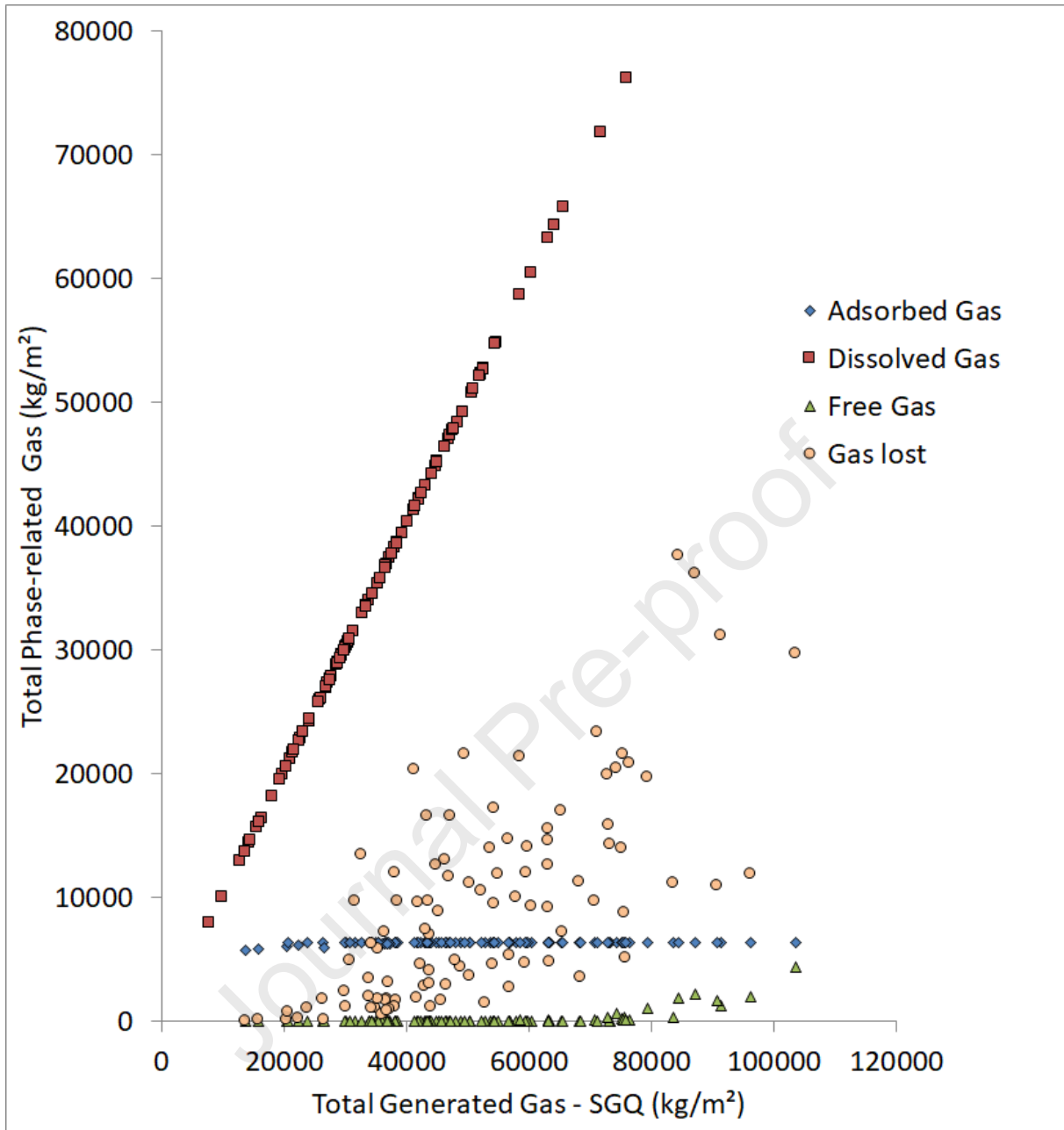
Figure 9. Microbial gas phase behavior as function of the total generated gas (SQG) based on a set of 100 simulations sampling the uncertain parameter space. The gas can be free in the system only when water becomes saturated. The total amount of gas lost at the surface increases as the cumulative generated gas increases.
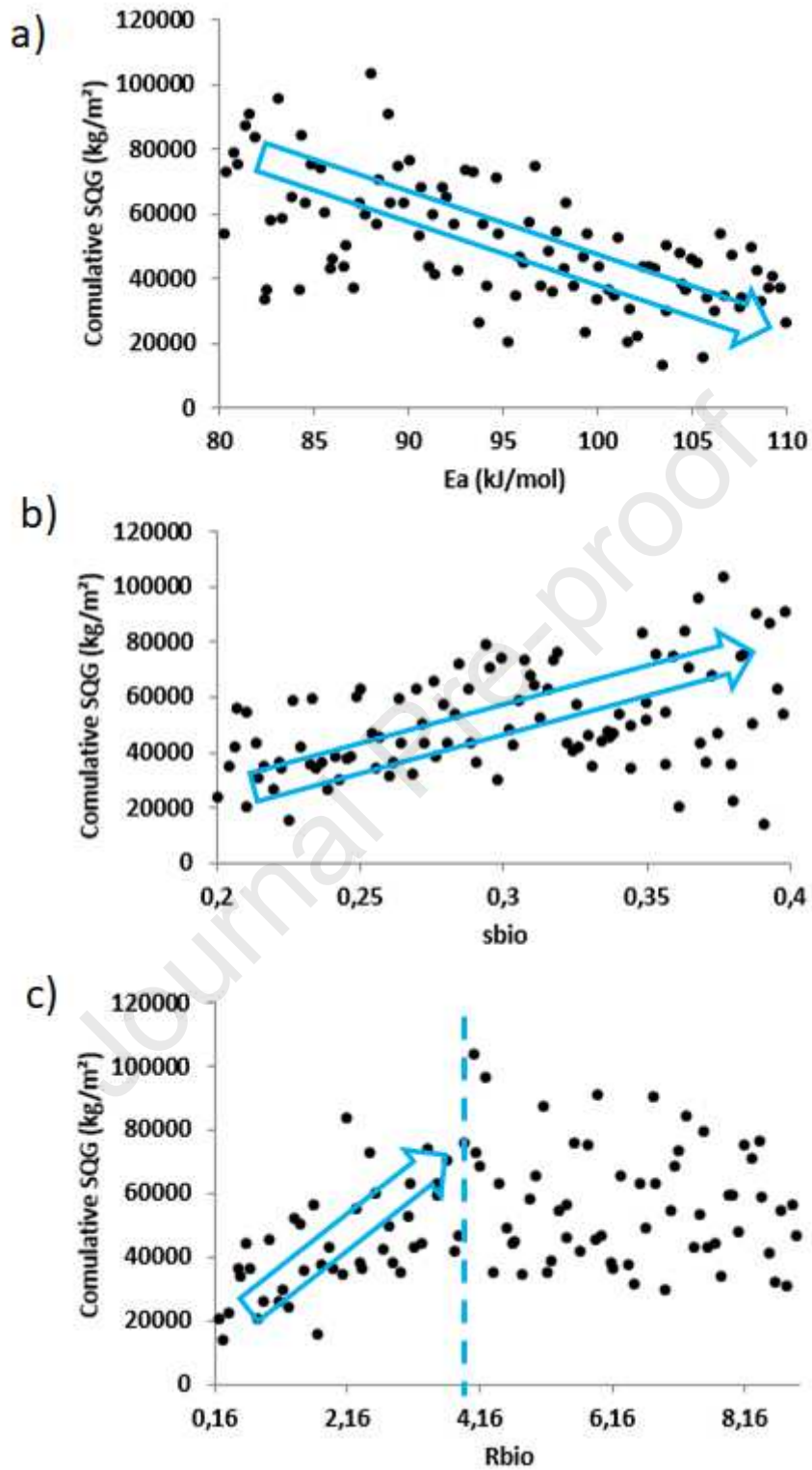
1208

1209

Figure 10. Total amount of generated gas (SQG) as function of three critical parameters for the 100 simulations of the training set. The SQG property shows some positive correlation with Sbio and some negative correlation with Ea. Some correlation is also visible for values of Rbio lower than 4. No clear trend can be observed between SQG and any other parameter.
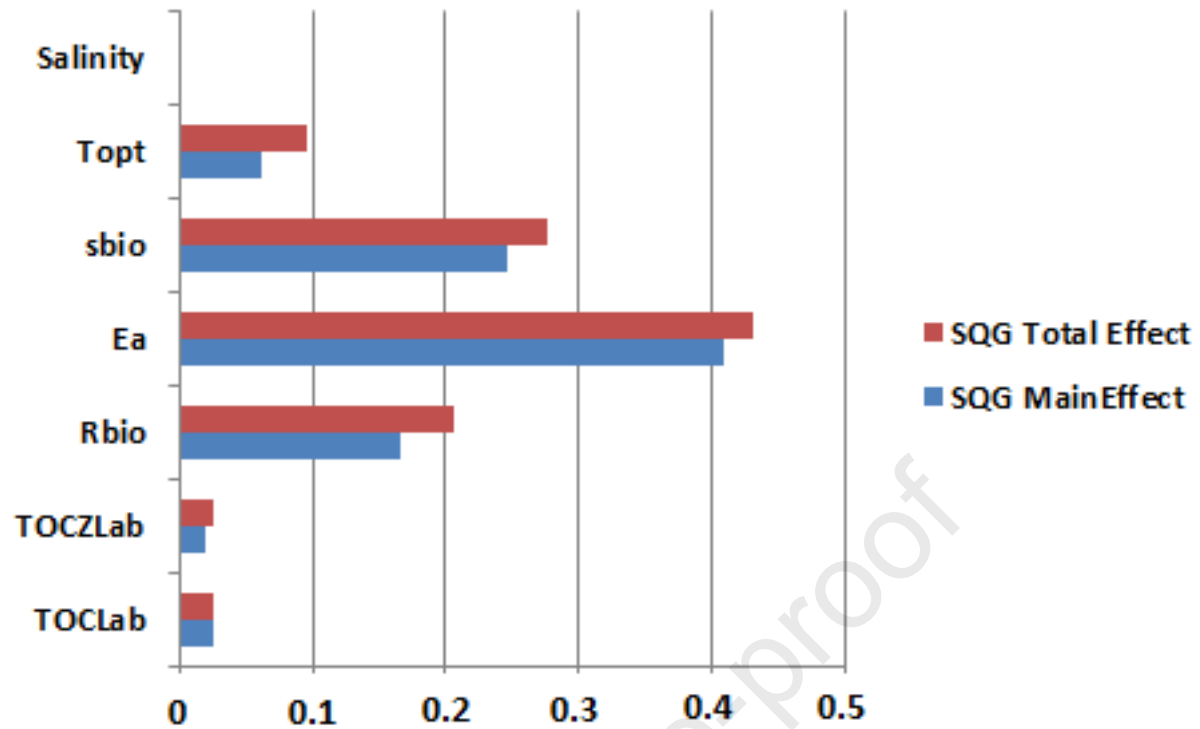
1214

Figure 11. Total and main effects on the total generated gas (SQG) computed for the 7 uncertain parameters. The small differences between the two effects highlight that, in our case study, there are no significant interactions between the parameters that affect the generation of methane. SQG is mainly impacted by Ea, s_{bio} and R_{bio} parameters, in order of priority.

1215
1216
1217
1218

1219
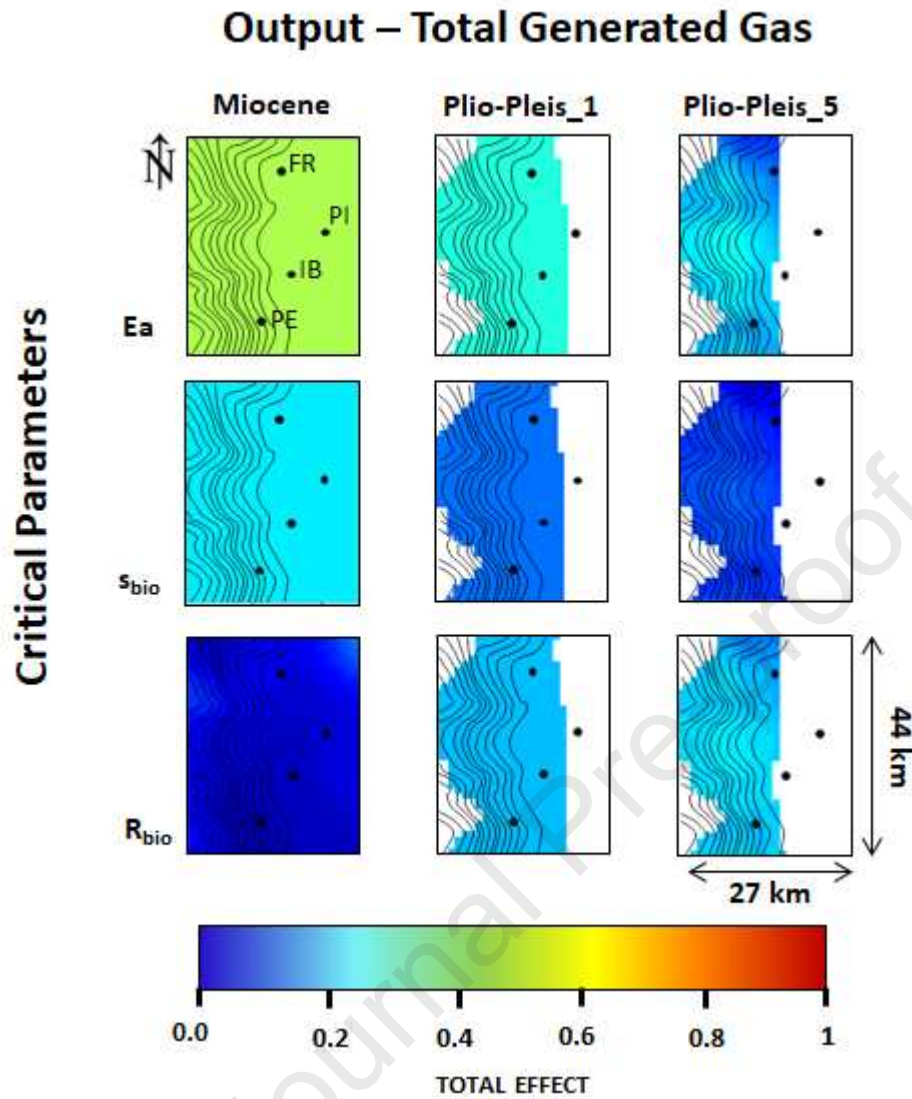
Figure 12. Total effect obtained for the three main influential parameters (Ea, s$_{bio}$, R$_{bio}$) on three of the six source rock layers (Table 3) over the northern studied area (see location in Fig. 1b). Black dots represent the offshore wells (FR – Fregate-1; PI – Pingouin-1; IB – Ibis-1; PE – Pelican-1) (Figs. 1, 3 and 5). Black lines represent the seafloor bathymetry with a contour interval of 50 m.
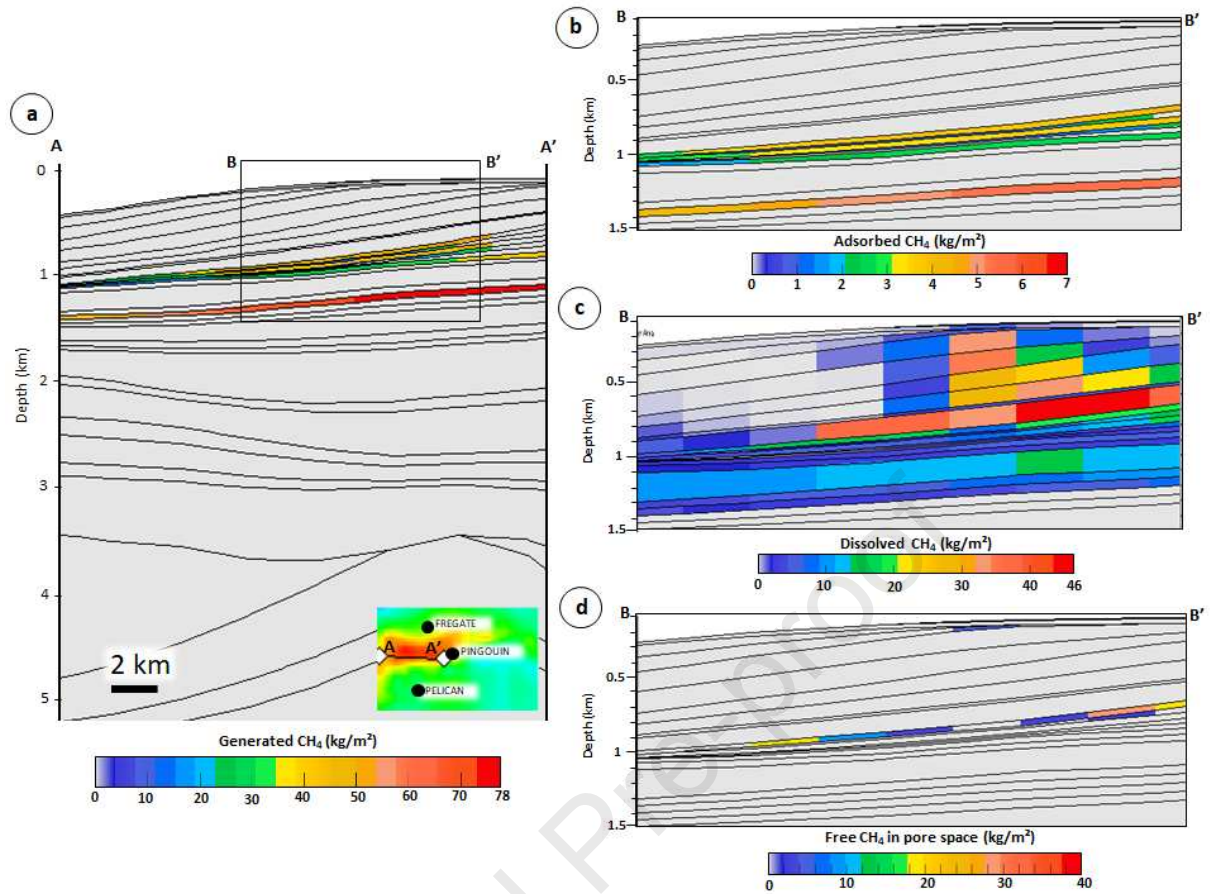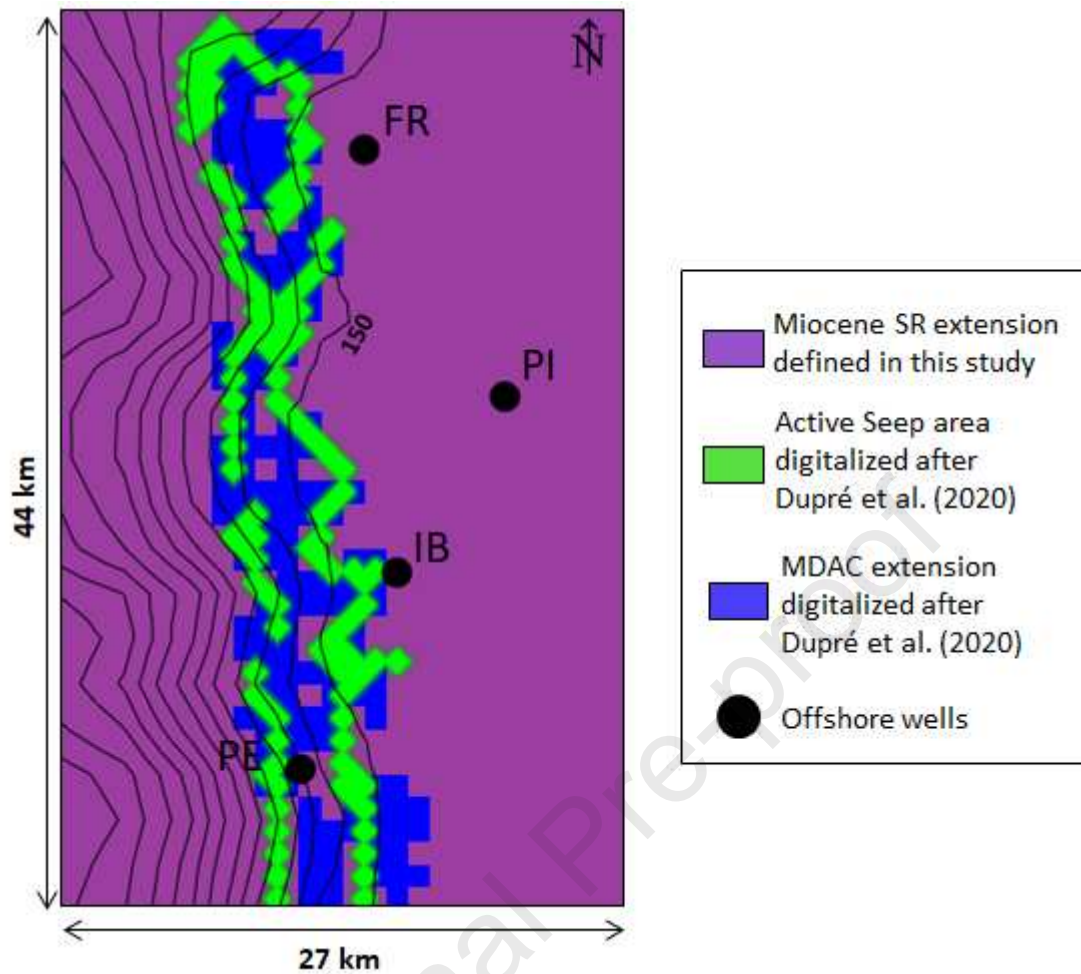
1230

Figure 13. 2D sections across the basin model (profile AA') showing mass of a) the generated gas from biogenic production per area and b-d) mass of gas in place per area at the present day, with b) total mass of gas adsorbed in the organic matter; c) total mass of gas dissolved in formation water; and d) total mass of free gas in pore space.

1234

1235

Figure 14. Map of Miocene Source Rock (SR) defined in this study with extent of seeps and MDACs digitized from Dupré et al. (2020) over the northern study area (see map location in Fig. 1b). The location of the offshore wells (FR – Fregate-1; PI – Pingouin-1; IB – Ibis-1; PE – Pelican-1) is given in Figs.1 and 3. Black lines represent the seafloor bathymetry with a contour interval of 50 m.
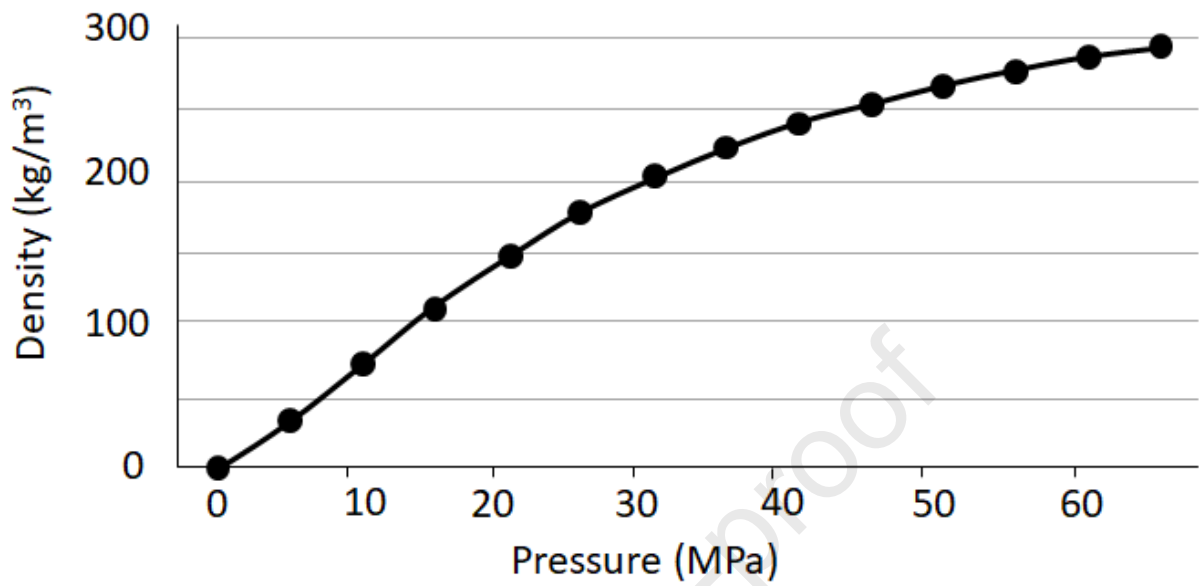
1251

1252

1253

1254 **Figure 15. Methane density as function of pressure using the AGA8 equation of state (ISO 12213-2, 2006; Starling and**
1255 **Savidge1992).**

1256

1257

1258

1259

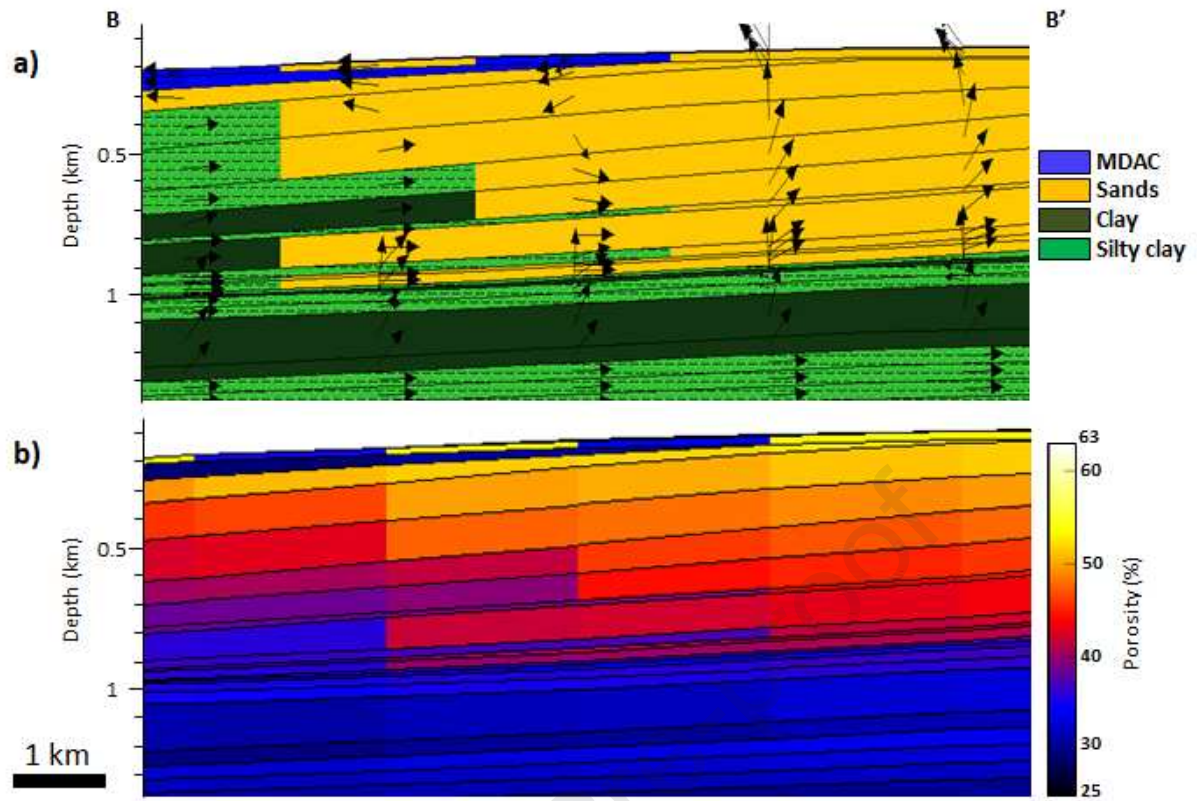1260

1261

1262

1263

1264

1265

1266

1267

1268

1269

1270

1271 **Figure 16. Modelled results along the 2D section B-B' shown in Figure 13. a) Facies distribution; b) Porosity (%). The**
1272 **black arrows show the water flow direction which is a function of facies and porosity.**

1273

1274

1275

1276

1277

1278

1279

1280
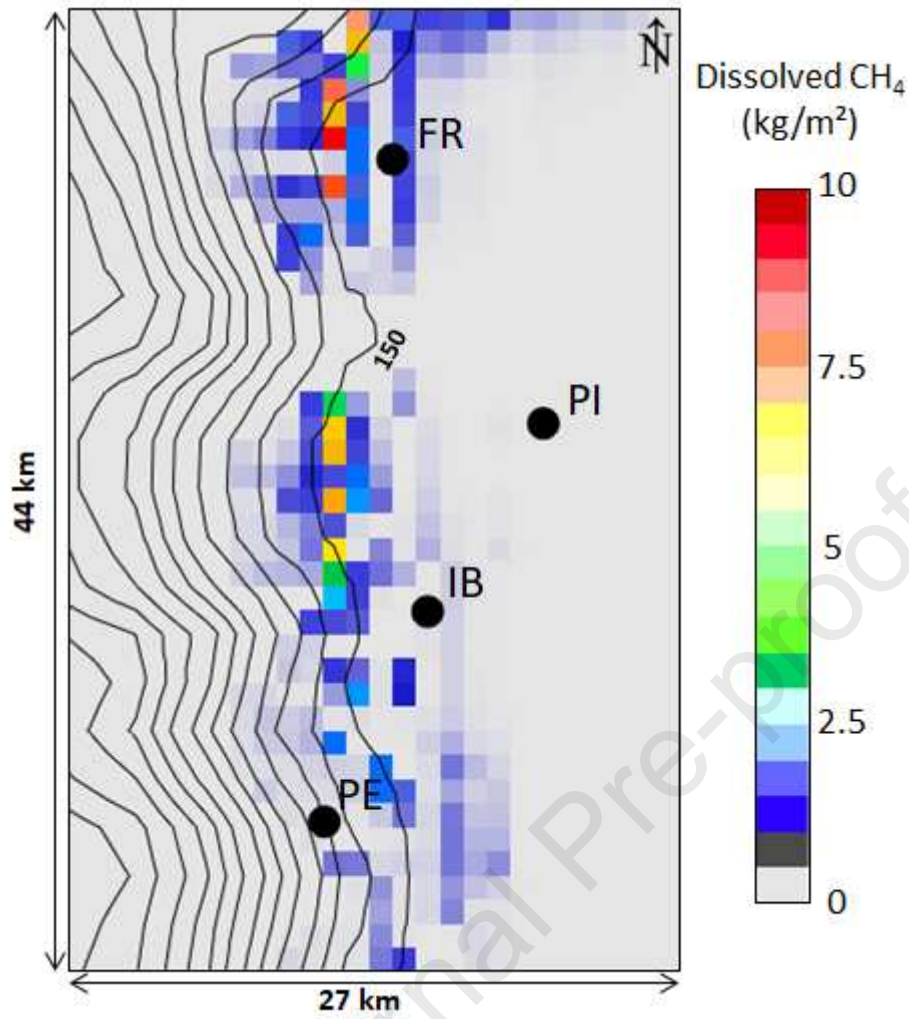
1281

Figure 17. Present-day modelled dissolved methane (kg/m²) in the second layer from top seafloor along the northern study area emission sites (for map location see Fig. 1b). Black dots indicate the offshorewells (FR – Fregate-1; PI – Pingouin-1; IB – Ibis-1; PE – Pelican-1) (Figs. 1, 3). Black lines represent the seafloor bathymetry with a contour interval of 50 m.

1286

1287

1288

1289

1290

1291

1292

1293

1294

1295

1296

1297 **Table 1. Geological layers and sub-layering for the main target area of biogenic gas generation. Interpreted seismic**
1298 **horizons are derived from OROGEN Project (Total) (Basement to Oligocene), Ortiz et al. (2020) (Miocene to Seabed),**
1299 **and Michel (2017) (Plio-Pleistocene units). The two uppermost layers are created by a lithoswitch to account for**
1300 **precipitation of MDACs during CH$_4$ upward migration.**

Top Age (Ma)	Layers	Interpreted Horizons from seismic	Sub-layering
0.0	MDAC		
0.14	Seabed	x	
0.25	Plio-Pleistocene U3	x	8 sub-layers
1.76	Plio-Pleistocene U2	x	7 sub-layers
3.53	Plio-Pleistocene U1	x	
5.30	Miocene	x	6 sub-layers
13.82	Langhian-Serravallian	x	
20.24	Aquitanian		
23.03	Oligocene	x	
33.90	Upper Eocene		
41.20	Lower Eocene		
56.00	Paleocene		
66.00	Upper Cretaceous	x	
100.50	Albian	x	
113.00	Aptian	x	
125.00	Barremian		
130.00	Neoconomian		
145.00	Top Jurassic	x	
175.60	Top Lias		
201.30	Top Triassic	x	
250.00	Top Basement	x	

1301

1302

1303

1304

1305

1306

1307

1308

1309

1310

1311

1312

1313

1314

1315

1316

1317 **Table 2. Range of parameters considered as uncertain in this study (Min and Max) and values selected for an optimal**
1318 **biogenic gas production ("This study").**

Input Parameter	Min	Max	This Study	Unit
TOClab	20	24	22	%
TOCzlab	15	19	19	%
Rbio	0.16	9	1.7	
Ea	80	110	83	kJ/mol
Sbio	0.2	0.4	0.35	
Salinity	40	60	50	g/L
$\mu(T)$	30	55	32	°C

1319

1320

1321

1322

1323

1324

1325

1326

1327

1328

1329

1330

1331

1332

1333

1334

1335

1336

1337

1338 **Table 3. Source rock age, modelled temperature and thermal conductivity. TOC bio-refractory (TOC$_{bio-ref}$) values are**
1339 **defined after the Rock-Eval analysis (Table S1).**

Source Rock	Top_Age	Mean Depth	Mean Temperature	Mean Thermal Conductivity	TOCbio-ref
	(Ma)	(m)	(°C)	(W/m.°C)	(%)
Plio-Pleis_5	1.76	585	14	1.60	0.49
Plio-Pleis_4	1.98	618	16	1.64	0.42
Plio-Pleis_3	2.20	670	17	1.66	0.44
Plio-Pleis_2	2.42	708	20	1.63	0.30
Plio-Pleis_1	2.87	823	22	1.61	0.29
Miocene	5.53	1100	30	1.54	0.51

1340

1341

1342

1343

1344

1345

1346

1347

1348

1349

1350

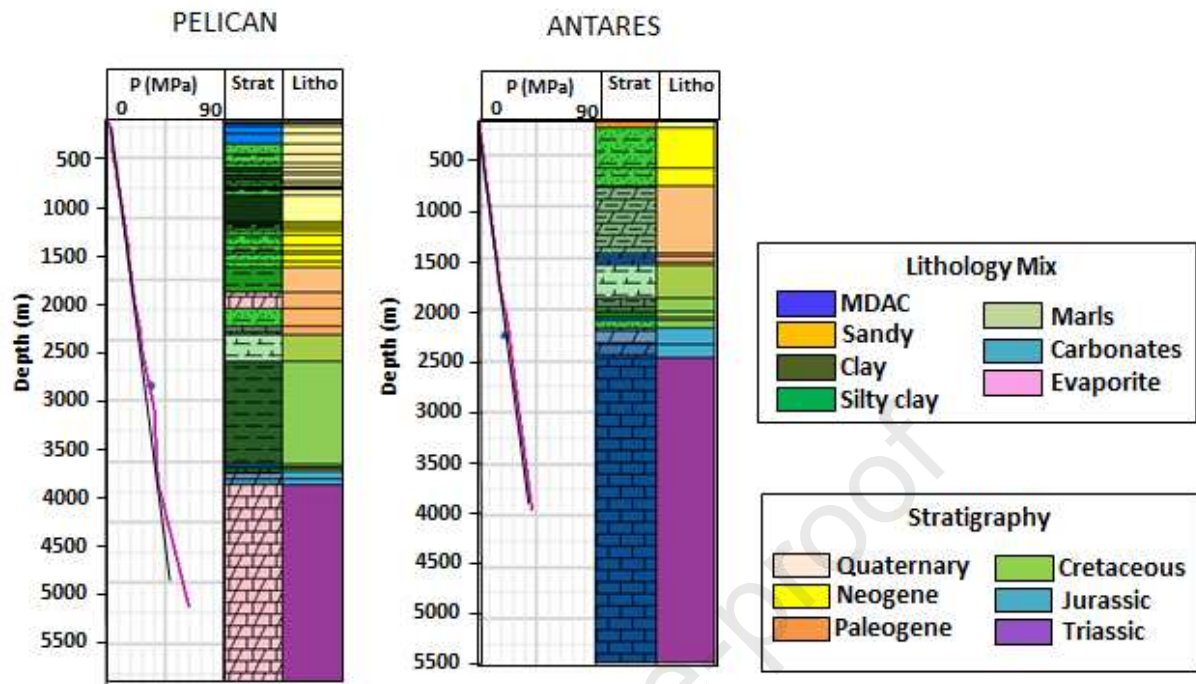1351

1352

1353

1354

1355

1356

1357

1358

1359

1360

1361 SUPPLEMENTARY MATERIAL:

1362

1363 **Figure S1. Pressure calibration for two wells. Well location is given in Fig. 3.**

1364 **Table S1. Rock-Eval results on cuttings collected from two offshore wells (Pingouin-1 and Pelican-1). Well locations**
1365 **are given in Fig. 3.**

Sample	Depth	S2	Tmax	HI	OI	TOC
	m	mgHc/g-rock	°C	mg Hc/g TOC	mg CO$_2$/g TOC	%
PINGOUIN-1	595	0.22	424	51	286	0.44
PINGOUIN-2	715	0.12	437	41	427	0.28
PINGOUIN-3	735	0.11	423	41	387	0.26
PINGOUIN-4	875	0.04	422	21	501	0.2
PINGOUIN-5	955	0.09	421	31	343	0.29
PINGOUIN-6	1025	0.11	420	39	334	0.29
PINGOUIN-7	1125	0.05	420	25	430	0.22
PINGOUIN-8	1145	0.14	420	39	292	0.35
PINGOUIN-9	1265	0.14	422	43	307	0.32
PINGOUIN-10	1325	0.15	421	47	279	0.32
PINGOUIN-11	1425	0.1	421	33	305	0.31
PELICAN-1	740	0.14	421	32	328	0.44
PELICAN-2	860	0.15	424	34	306	0.44
PELICAN-3	960	0.19	424	38	290	0.49
PELICAN-4	1050	0.19	422	43	292	0.46
PELICAN-5	1200	0.1	422	27	321	0.36
PELICAN-6	1280	0.15	439	36	387	0.41
PELICAN-7	1493	5.67	432	55	106	10.35
PELICAN-8	1500	0.21	421	38	238	0.53
PELICAN-9	1530	0.2	420	43	284	0.47

1366

1367

1368

1369

1370

1371

HIGHLIGHTS

- Innovative 3D basin modelling approach to quantify the budget of biogenic methane in continental shelf areas and calibrated to sea floor emissions

- Sensitivity analysis to determine impact of main parameters on biogenic gas generation and expulsion/migration processes in offshore Aquitaine

- Quantification of methane consumed and stored in authigenic carbonates as function of efficiency of AOM (Anaerobic Oxidation of Methane)

- Methane migration is diffuse and mainly vertical from the source rock layers to the seafloor dissolved in pore water

- Biogenic methane is sourced by an active system with a maximum flow rate modelled during the early Pleistocene

Declaration of interests

☒ The authors declare that they have no known competing financial interests or personal relationships that could have appeared to influence the work reported in this paper.

☐The authors declare the following financial interests/personal relationships which may be considered as potential competing interests: